

General Theory of Stable Microwave-Optical Quantum Resources in Hybrid-System Dynamics

Fan Li,¹ Shi-fan Qi,^{1,*} Z. D. Wang,^{2,3,†} and Yan-Kui Bai^{1,3,‡}

¹*College of Physics and Hebei Key Laboratory of Photophysics Research and Application,
Hebei Normal University, Shijiazhuang, Hebei 050024, China*

²*HK Institute of Quantum Science & Technology and Department of Physics,
The University of Hong Kong, Pokfulam Road, Hong Kong, China*

³*Hong Kong Branch for Quantum Science Center of Guangdong-Hong Kong-Macau Greater Bay Area, Shenzhen 518045, China*

We develop a general theoretical framework for characterizing stable quantum resources between microwave and optical modes in the dynamics of multipartite hybrid quantum systems with intermediary modes. The effective Hamiltonian for microwave-optical (MO) squeezing is formulated via strong interactions in the microwave-intermediary-optical hybrid system, and based on which rigorous solutions for the dynamics of MO entanglement and quantum steering are derived analytically. Remarkably, it is found that stable MO quantum resources can survive in the unsteady evolution beyond the steady one, and the unsteady evolution can exhibit the enhanced quality over the limit of quantum resources in the steady-state case. Furthermore, the stable MO entanglement as well as one-way and two-way quantum steerings are efficiently controllable by modulating the effective coupling strength. The validity of our theory is demonstrated by applying it to the typical models of electro-optomechanical and cavity optomagnomechanical hybrid systems.

Introduction.—Microwave and optical modes play distinct roles in quantum technologies [1–7], where the former facilitates quantum control of various physical systems [8, 9] and the latter is capable of long-distance information propagation [10, 11]. Efficient conversions between these two modes [12–19] are indispensable in distributed quantum information processing toward a future quantum internet [20–23]. Based on microwave-optical (MO) nonlocal resources such as entanglement [24] and quantum steering [25], the indirect transduction [26, 27] is an alternative and promising approach which has the merits of high transfer efficiency and favorable noise tolerance [28, 29]. Therefore, the generation of stable MO quantum resources is a fundamental problem, which typically requires the intermediate modes in hybrid multipartite systems due to the large frequency mismatch between microwave and optical modes [12, 13]. Under steady-state conditions, significant progress on generation of MO quantum resources have been made based on various hybrid multipartite systems, including electro-optomechanical systems [26, 30–35], cavity optomagnomechanical systems [36–39], magneto-optomechanical systems [40, 41], and so on.

The inherent configuration complexity of multipartite hybrid systems poses a significant challenge for the analytical study of the MO nonlocal quantum resources, which can be used for high-precision control over entanglement and quantum steering in the MO quantum interface. Moreover, the MO entanglement and quantum steering cannot be freely shared in multipartite hybrid systems since entanglement and quantum steering are monogamous [42–49], and thus the analytical investigation on MO quantum resources generation can facilitate the multi-parameter optimization. On the other hand, the generation of nonlocal quantum resources in multipartite hybrid systems is a typical dynamical process [50–55]. Previous studies have demonstrated that two-qubit quantum correlations rather than entanglement do not decay in certain dynamical decoherence [56–58]. However, beyond the schemes based on the steady-state, it is still an open question whether

the stable MO entanglement and quantum steering can be generated in the unsteady-state dynamics. Recently, a theoretical study has indicated that transient optoacoustic entanglement can be generated during the dynamical process of unsteady state [59], which further motivates the investigation into the generation of stable MO quantum resources in the unsteady-state dynamics.

In this Letter, we propose a general approach to generate MO entanglement and quantum steering of the two non-interacting modes by constructing an effective two-mode squeezing coupling assisted by chain-coupled intermediate modes. Based on the effective two-mode squeezing Hamiltonian, the system dynamics governed by the quantum Langevin equations within the open-quantum-system framework can be solved analytically. Furthermore, the analytical formulas of MO entanglement and quantum steering are obtained, which facilitates precise control of these nonlocal quantum resources by modulating the effective coupling strength. It is found that the stable MO quantum resources can survive in the unsteady-state dynamics and are stronger than those in the steady case. Finally, the validity of our theory is verified in two typical models of electro-optomechanical [26, 31] and cavity optomagnomechanical hybrid systems [36].

General theory for MO chain-type systems.—As shown in Fig. 1, we consider a multipartite hybrid system consisting of microwave mode a , optical mode c , and chain-type N -

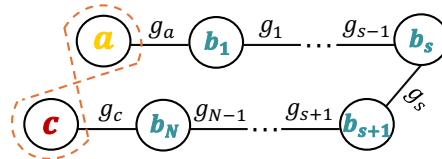


FIG. 1. Diagram of a multipartite hybrid system consisting of two target modes (microwave mode a and optical mode c) and chain-type N -intermediate modes (b_1, b_2, \dots, b_N). The adjacent couplings are represented by g_a , g_c , and g_s with $s = 1, 2, \dots, N - 1$.

intermediate modes b_1, b_2, \dots, b_N . Without loss of generality, the hybrid system Hamiltonian in the interaction picture may be expressed as ($\hbar \equiv 1$)

$$\begin{aligned} H &= H_0 + V, \\ H_0 &= \Delta_a a^\dagger a + \Delta_c c^\dagger c + \sum_{s=1}^N \omega_s b_s^\dagger b_s, \\ V &= V_a + V_b + V_c, \\ V_a &= g_a [\cos \theta (a^\dagger b_1 + a b_1^\dagger) + \sin \theta (a^\dagger b_1^\dagger + a b_1)], \\ V_b &= \sum_{s=1}^{N-1} g_s (b_s + b_s^\dagger) (b_{s+1} + b_{s+1}^\dagger), \\ V_c &= g_c [\cos \phi (c^\dagger b_N + c b_N^\dagger) + \sin \phi (c^\dagger b_N^\dagger + c b_N)]. \end{aligned} \quad (1)$$

Here, a (a^\dagger), b_s (b_s^\dagger), and c (c^\dagger) are the annihilation (creation) operators of the modes a , b_s , and c , respectively. Δ_a and Δ_c are the frequency detunings of target modes a and c with respect to the lab frame, and ω_s is the transition frequency of mode b_s . g_a , g_s , and g_c are corresponding coupling strengths between the adjacent modes, and the angles θ and ϕ parameterize the magnitude of rotating and counter-rotating couplings between modes a and b_1 , c and b_N , respectively. This MO hybrid model in Eq. (1) is realizable in various physical platforms with different intermediate modes, such as the electro-optomechanical system [26, 30, 31] ($N = 1$), the cavity optomagnomechanical system [36, 37] ($N = 2$), and the magneto-optomechanical system [40, 41] ($N = 3$).

Our theoretical framework for MO quantum resources is derived from engineering an effective two-mode squeezing interaction between microwave mode a and optical mode c assisted by auxiliary modes b_s . Using a generalized analysis of virtual transition pathways on the full Hamiltonian in Eq. (1) by the nearly degenerate perturbation theory [60–63], we can obtain the effective Hamiltonian

$$H_{\text{eff}} = g_{\text{eff}} (a^\dagger c^\dagger + a c), \quad (2)$$

where g_{eff} is the effective coupling strength, and we employ the conditions $g_a, g_s, g_c \ll \{|\Delta_a - \omega_s|, |\Delta_c - \omega_s|\}$ and $\Delta_a = -\Delta_c + \delta$ with δ being the energy shift. The rigorous derivation for H_{eff} in Eq. (2) is presented in End Matter, where the analytical formula of effective coupling strength g_{eff} for arbitrary number of intermediate modes is given in Eq. (A4). The resulting effective Hamiltonian simplifies the complex multipartite hybrid system into the MO subsystem, allowing for a more rigorous investigation on the dynamics of MO quantum resources.

According to the effective Hamiltonian in Eq. (2), the evolution of MO subsystem in the open-quantum-system framework can be analytically derived via the quantum Langevin equations [64]. Given that the initial state is Gaussian, the dynamics of MO quantum system in a Markovian environment can be fully characterized by a 4×4 covariance matrix (CM) $v(t)$ [52, 53], which satisfies

$$\dot{v}(t) = A_{\text{eff}} v(t) + v(t) A_{\text{eff}}^T + D_{\text{eff}}, \quad (3)$$

where $\dot{v}(t)$ denotes the derivation of $v(t)$. The elements of $v(t)$ are defined as $v_{ij}(t) = \langle u_i(t) u_j(t) + u_j(t) u_i(t) \rangle / 2 - \langle u_i(t) \rangle \langle u_j(t) \rangle$ ($i, j = 1, 2, 3, 4$), where $u_i(t)$ is the i -term of $u(t) = [X_a(t), Y_a(t), X_c(t), Y_c(t)]^T$ and $X_o = (o + o^\dagger)/\sqrt{2}$, $Y_o = (o - o^\dagger)/i\sqrt{2}$, $o = a, c$. Moreover, the drift matrix A_{eff} in Eq. (3) has the form

$$A_{\text{eff}} = - \begin{pmatrix} \kappa_a & 0 & 0 & g_{\text{eff}} \\ 0 & \kappa_a & g_{\text{eff}} & 0 \\ 0 & g_{\text{eff}} & \kappa_c & 0 \\ g_{\text{eff}} & 0 & 0 & \kappa_c \end{pmatrix}, \quad (4)$$

where κ_a and κ_c represent the decay rates of the modes a and c , respectively, and $D_{\text{eff}} = \text{diag}[\kappa_a, \kappa_a, \kappa_c, \kappa_c]$ is the diffusion matrix. At the initial time, it is assumed that two target modes are in the vacuum state $v(0) = I_4/2$ with I_4 being the identity matrix of four dimensions. After substituting Eq. (4) into Eq. (3), we can obtain the CM

$$v(t) = \begin{pmatrix} v_{11}(t) & 0 & 0 & v_{14}(t) \\ 0 & v_{11}(t) & v_{14}(t) & 0 \\ 0 & v_{14}(t) & v_{44}(t) & 0 \\ v_{14}(t) & 0 & 0 & v_{44}(t) \end{pmatrix}, \quad (5)$$

where the analytical expressions of the non-zero matrix elements and the detailed derivation of $v(t)$ are provided in Sec. IA of the Supplement Material (SM) [65]. When the effective coupling strength satisfies $g_{\text{eff}}^2 < \kappa_a \kappa_c$, the MO system evolves toward a steady state obtained by $\dot{v}(t) = 0$. Conversely, when $g_{\text{eff}}^2 \geq \kappa_a \kappa_c$, the target system undergoes the unsteady state evolution and the matrix $v(t)$ exhibits divergent behavior.

The stable MO quantum resources.—According to the analytical expression of $v(t)$ in Eq. (5), we are able to study the MO dynamics and calculate the targeted entanglement and quantum steering at any given time. We use the logarithmic negativity [66–69] to quantify the two-mode MO entanglement

$$E_{ac}(t) = \max[0, -\ln(2\eta_{ac}^-)], \quad (6)$$

where η_{ac}^- is the minimum symplectic eigenvalue of the partial transpose matrix of the CM $v(t)$. In the dynamical evolution of MO subsystem, the two-mode entanglement $E_{ac}(t)$ at $t \rightarrow \infty$ will converge to a fixed value

$$E_{ac} = \begin{cases} \ln \left(\frac{\kappa_a \kappa_c - g_{\text{eff}}^2}{\kappa_a \kappa_c - g_{\text{eff}}^2 \chi} \right), & g_{\text{eff}}^2 < \kappa_a \kappa_c \\ \ln \left(1 + 4 \frac{g_{\text{eff}}^2}{\tilde{\chi}} \right), & g_{\text{eff}}^2 \geq \kappa_a \kappa_c \end{cases} \quad (7)$$

where the piecewise function corresponds to the stable MO entanglement for the steady-state and unsteady-state cases, respectively, and the parameters are $\chi = \{1 + 4\kappa_a \kappa_c (\kappa_a \kappa_c - g_{\text{eff}}^2) / [g_{\text{eff}}^2 (\kappa_a + \kappa_c)^2]\}^{1/2}$ and $\tilde{\chi} = \Omega(\kappa_a + \kappa_c) + (\kappa_a - \kappa_c)^2$ with $\Omega = [4g_{\text{eff}}^2 + (\kappa_a - \kappa_c)^2]^{1/2}$. For the given decay rates κ_a and κ_c , the stable MO entanglement E_{ac} in Eq. (7) is

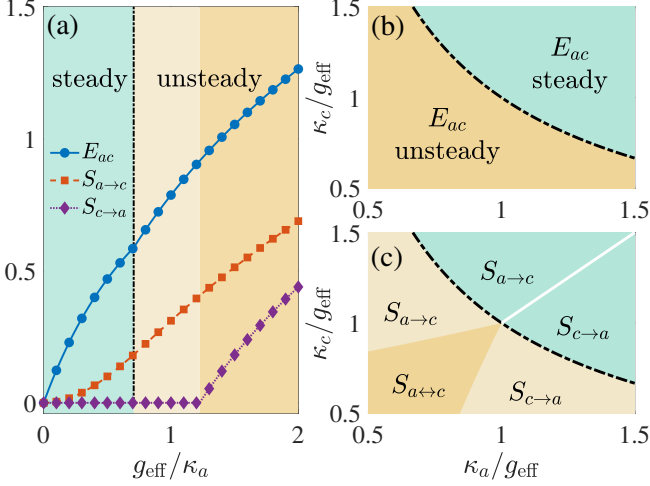


FIG. 2. The control of MO quantum resources via effective parameters. (a) The MO entanglement E_{ac} (the blue line), asymmetric quantum steerings $S_{a\rightarrow c}$ (the red line) and $S_{c\rightarrow a}$ (the purple line) along with the relative coupling g_{eff}/κ_a for the decay rates $\kappa_c = 2\kappa_a = 1$. (b) The regional diagram of MO entanglement E_{ac} for the steady-state (the teal area) and the unsteady-state (the golden-yellow area) cases. (c) The regional diagram of asymmetric quantum steering for the steady-state case (the two teal areas for $S_{a\rightarrow c}$ and $S_{c\rightarrow a}$ with the white boundary being zero value) and the unsteady-state case (the two beige areas for the asymmetric one-way steerings and the golden-yellow area for the two-way steering $S_{a\leftrightarrow c}$). The black dot-dashed line indicates the boundary between the steady-state and unsteady-state dynamics in the three panels, and the effective coupling strength is $g_{\text{eff}} = 1$ in (b) and (c).

monotonically increasing along with the square of effective coupling strength g_{eff}^2 , and the piecewise E_{ac} is continuous as $g_{\text{eff}}^2 \rightarrow (\kappa_a \kappa_c)^-$. The derivation of Eq. (7) and analysis of related properties are presented in Sec. IB of the SM [65].

Quantum steering of continuous variables is a kind of asymmetric quantum resource [25], and can enable one-sided device-independent quantum key distribution [70–72] and random number generation [73, 74]. Based on the analytical CM $v(t)$ in Eq. (5), the two-mode steering from a to c under Gaussian measurements [75] can be quantified by

$$S_{a\rightarrow c}(t) = \max[0, S_{ac}], \quad (8)$$

where the quantity $S_{ac} = \ln[\det v_a / (4 \det v)]/2$ with v_a being the CM of the microwave mode a . In the dynamical process at $t \rightarrow \infty$, the quantity S_{ac} evolves to a stationary value

$$S_{ac} = \begin{cases} \ln \left[\frac{g_{\text{eff}}^2(\kappa_c^2 - \kappa_a^2) + \Xi}{g_{\text{eff}}^2(\kappa_a - \kappa_c)^2 + \Xi} \right], & g_{\text{eff}}^2 < \kappa_a \kappa_c \\ \ln \left(\frac{\Omega - \kappa_a + \kappa_c}{2\Omega} \right) + E_{ac}, & g_{\text{eff}}^2 \geq \kappa_a \kappa_c \end{cases} \quad (9)$$

where the piecewise function corresponds to the steady-state and unsteady-state evolutions, respectively. The parameters are $\Xi = \kappa_a \kappa_c (\kappa_a + \kappa_c)^2$, $\Omega = [4g_{\text{eff}}^2 + (\kappa_a - \kappa_c)^2]^{1/2}$, and

E_{ac} is the fixed value of the unsteady-state entanglement in Eq. (7). The nonzero steering $S_{a\rightarrow c}(\infty)$ arises, when the conditions $g_{\text{eff}}^2 > 0$ for $\kappa_a < \kappa_c$ and $g_{\text{eff}}^2 > \kappa_a(2\kappa_a - \kappa_c)$ for $\kappa_a \geq \kappa_c$ are satisfied. The asymmetric one-way steering $S_{c\rightarrow a}(t)$ from mode c to mode a has a similar formula as those in Eqs. (8) and (9) by interchanging the decay rates κ_a and κ_c . Moreover, the stable two-way steering $S_{a\leftrightarrow c}(\infty)$ only exists in the unsteady-state evolution, and the system parameters need to satisfy the condition $g_{\text{eff}}^2 + \kappa_a \kappa_c > 2\kappa_a^2, 2\kappa_c^2$. For the given decay rates κ_a and κ_c , the stationary values at $t \rightarrow \infty$ of $S_{a\rightarrow c}$ and $S_{c\rightarrow a}$ are monotonically increasing along with the square of effective coupling strength g_{eff}^2 , the values of stable asymmetric steerings are smaller than that of stable entanglement E_{ac} . Details of the derivation of Eq. (9) and the analysis of related properties are presented in Sec. IC of the SM [65].

These stable quantum resources can be quantitatively controlled by modulating the effective coupling strength g_{eff} and the decay rates κ_a and κ_c in terms of the corresponding analytical expressions of entanglement and quantum steering. As shown in Fig. 2, the control of MO quantum resources via the effective parameters is plotted. In Fig. 2(a), the stable entanglement E_{ac} , one-way quantum steerings $S_{a\rightarrow c}$ and $S_{c\rightarrow a}$ are plotted along with the increasing of relative coupling strength g_{eff}/κ_a with the decay rates being $\kappa_c = 2\kappa_a = 1$. The nonzero quantum resources are increasing along with the effective coupling strength, and the value of entanglement E_{ac} is larger than those of steerings $S_{a\rightarrow c}$ and $S_{c\rightarrow a}$ indicating the higher requirements for generation of one-way and two-way quantum steerings. The regional diagram for stable MO entanglement E_{ac} is illustrated in Fig. 2(b), where the teal area denotes the steady-state case and the golden-yellow area corresponds to the entanglement in the unsteady-state evolution. In Fig. 2(c), the regional diagram for asymmetric steering is provided, where the two teal areas represent the nonzero one-way steerings $S_{a\rightarrow c}$ and $S_{c\rightarrow a}$ of the steady-state case with zero steering for $\kappa_a = \kappa_c$ (the white line), the two beige areas denote two asymmetric one-way steerings in the unsteady-state dynamics, and the golden-yellow area indicates the two-way steering $S_{a\leftrightarrow c}$ for the unsteady-state case.

Application in MO hybrid systems.—For a concrete MO hybrid system, the effective Hamiltonian corresponding to Eq. (2) can be constructed by the method presented in the End Matter. Then we are able to obtain the rigorous expressions of g_{eff} and the stable quantum resources via the analytical CM $v(t)$ in Eq. (5). In the dynamics of the MO system, we introduce a characteristic time τ to indicate the moment that the evolution values of entanglement and quantum steerings are nearly identical to the analytical stationary values at $t \rightarrow \infty$ given in Eqs. (7) and (9), which is defined as

$$\tau = \frac{4\pi}{\Omega + \kappa_a + \kappa_c}, \quad (10)$$

where the parameter Ω is a function of effective coupling strength g_{eff} and the decay rates κ_a and κ_c [65]. The validity of our developed analytical approach can be confirmed by

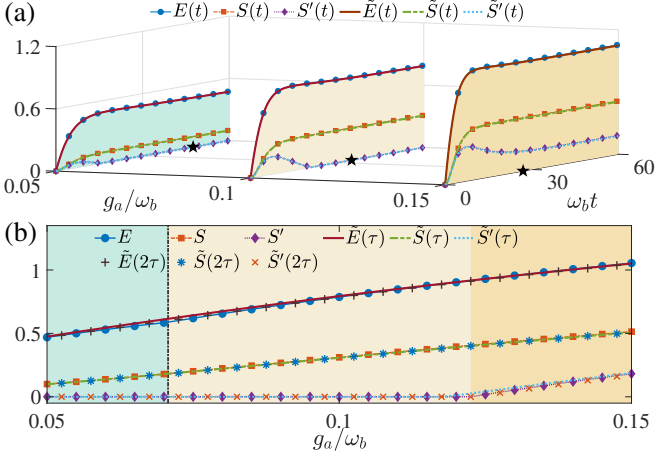


FIG. 3. The stable MO entanglement and quantum steerings in the EOM system. (a) The steady-state (the teal region) and unsteady-state (the beige and golden-yellow regions) dynamics of MO quantum resources for three typical values of coupling strength g_a/ω_b with the star symbols indicating the characteristic time τ . (b) The stationary values of MO quantum resources along with the coupling g_a , coinciding with the results of the full system dynamics at $t = \tau$ and $t = 2\tau$. The MO entanglement is represented by E , the steering from mode a to c is denoted S , and the one from c to a is represented by S' . The quantities with a tilde are the results of full system dynamics. The system parameters are $g_c = 0.12\omega_b$, $\Delta_a = 5\omega_b$, $\kappa_c = 0.5\kappa_a = 10^{-3}\omega_b$, $\kappa_b = 10^{-6}\omega_b$, and the thermal occupation numbers are $N_a = N_c = 0$, $N_b = 10$.

numerical verification via the full system dynamics governed by the multipartite Hamiltonian in Eq. (1).

Case 1: The electro-optomechanical system.—We first consider the generation of stable MO entanglement and quantum steerings in a multipartite hybrid electro-optomechanical (EOM) system [26, 31], where a mechanical mode b serves as an interface to couple the microwave mode a and the optical mode c . After some derivation [65], we can obtain the linearized multipartite Hamiltonian

$$H_{S_1} = \omega_b b^\dagger b + \sum_{o=a,c} \Delta_o o^\dagger o + g_o (o + o^\dagger)(b + b^\dagger), \quad (11)$$

where ω_b is the transition frequency, Δ_o denotes the detuning of mode o , and g_o represents the coupling strength between the mode o and the mechanical mode b with $o = a, c$. In comparison with general chain-type Hamiltonian in Eq. (1), the EOM Hamiltonian in Eq. (11) corresponds to $\theta = \phi = \pi/4$ and $N = 1$. Then, we construct the effective Hamiltonian H_{eff} in Eq. (2) for the EOM system by the perturbation theory [65], where the effective coupling strength has the form

$$g_{\text{eff}} = \frac{2g_a g_c \omega_b}{\Delta_a^2 - \omega_b^2}. \quad (12)$$

After substituting this analytical expression into the CM $v(t)$ in Eq. (5), we can derive the dynamical MO quantum resources $E_{ac}(t)$, $S_{a \rightarrow c}(t)$, $S_{c \rightarrow a}(t)$ and the stationary values

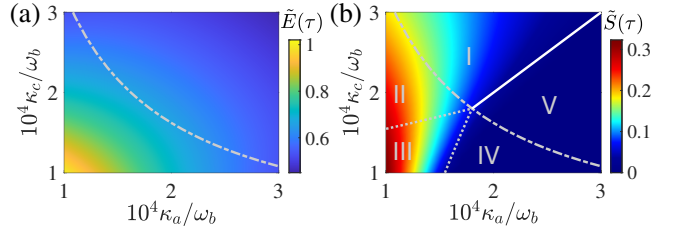


FIG. 4. The regional diagram of stable MO quantum resources in the COMM system. (a) The stable MO entanglement $\tilde{E}_{ac}(\tau)$ in the steady-state and unsteady-state evolutions with the white dot-dashed line being the boundary. (b) The stable MO quantum steering $\tilde{S}_{a \rightarrow c}(\tau)$ in two kinds of dynamical processes, where the regional map derived by the effective Hamiltonian method is well reproduced by the numerical results of full COMM-system dynamics. The parameters are set as $g_a = g_c = 0.12\omega_b$, $g_m = 0.1\omega_b$, $\Delta_a = 3\omega_b$, $\kappa_m = 10^{-3}\omega_b$, $\kappa_b = 10^{-6}\omega_b$, $N_a = N_c = N_m = 0$, and $N_b = 10$.

E_{ac} , $S_{a \rightarrow c}$, $S_{c \rightarrow a}$ in Eqs. (7) and (9) at $t \rightarrow \infty$. In the meantime, we perform the numerical full EOM-system dynamics governed by Eq. (12), which yields the time-dependent $\tilde{E}_{ac}(t)$, $\tilde{S}_{a \rightarrow c}(t)$, and $\tilde{S}_{c \rightarrow a}(t)$ to validate our analytical approach [65]. In Fig. 3(a), we plot the dynamical process of MO quantum resources for three typical coupling strengths ($g_a/\omega_b = 0.05, 0.1, \text{ and } 0.15$), where the results based on our effective Hamiltonian method exhibit the good agreements with those obtained by the numerical full EOM-system dynamics. Moreover, the dynamical values of quantum resources stabilize before the characteristic time τ (the star symbols). In Fig. 3(b), the stationary values of quantum resources in terms of analytical expressions in Eqs. (7) and (9) are plotted as g_a increases, which have good agreements with the numerical results at times τ and 2τ obtained by the full system dynamics and further validate the generation of stable quantum resources under both the steady-state and unsteady-state evolutions (see Sec. II in the SM [65]).

Case 2: The cavity optomechanical system.—A YIG crystal is placed inside a microwave cavity (mode a) to excite the magnon mode m , while simultaneously serving as the vibrating end mirror (mechanical mode b) of the optical cavity (mode c) [36]. For this cavity optomechanical (COMM) system, we can derive its linearized Hamiltonian

$$H_{S_2} = \sum_{o=a,m,c} \Delta_o o^\dagger o + \omega_b b^\dagger b + g_a (a^\dagger m + a m^\dagger) + \sum_{o=m,c} g_o (o + o^\dagger)(b + b^\dagger), \quad (13)$$

where ω_b is the transition frequency, g_{os} are the coupling strengths, and Δ_o s are the detunings [65]. This COMM system corresponds to the chain-type Hamiltonian in Eq. (1) for $\theta = 0$, $\phi = \pi/4$ and $N = 2$. After constructing the H_{eff} in Eq. (2) for the COMM system [65], we have

$$g_{\text{eff}} = \frac{2g_a g_m g_c \omega_b}{(\Delta_m - \Delta_a)(\omega_b^2 - \Delta_a^2)}, \quad (14)$$

which can be used to analytically describe the MO dynamics.

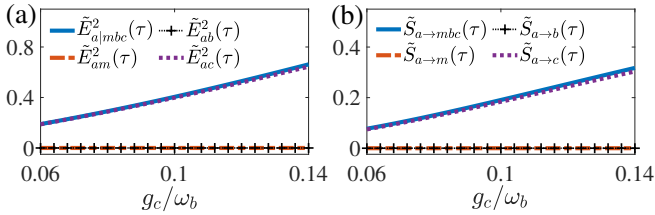


FIG. 5. The efficient quantum control over the MO entanglement (a) and quantum steering (b) in the COMM system, where the decay rates are $\kappa_a = 0.5\kappa_c = 10^{-4}\omega_b$ and other parameters have the same values as those in Fig. 4.

In Fig. 4, we plot the MO entanglement $\tilde{E}_{ac}(\tau)$ and quantum steering $\tilde{S}_{a \rightarrow c}(\tau)$ along with the relative decay rates of microwave and optimal modes at the characteristic time τ , where both the dynamical stationary values and the regional map (the boundaries for the steady-state and unsteady-state evolution as well as different asymmetric areas) derived by the effective Hamiltonian method are well reproduced by the numerical results by full COMM-system dynamics [65]. Moreover, the dynamical resources $\tilde{E}_{ac}(2\tau)$ and $\tilde{S}_{a \rightarrow c}(2\tau)$ are nearly identical to those at the time τ and coincide with the stationary values in terms of the analytical expressions in Eqs. (7) and (9), indicating the generation of stable quantum resources (see Sec. III in the SM [65]).

Discussion and conclusion.—Based on our developed effective Hamiltonian approach, we can realize the multi-parameter optimization for generation of the MO resources, which is manifested via the quantitative monogamy inequalities [46–49]. For example, in the COMM system, the entanglement and quantum steering distributions satisfy

$$\begin{aligned} \tilde{E}_{a|m b c}^2 &\geq \tilde{E}_{ac}^2 + \tilde{E}_{ab}^2 + \tilde{E}_{am}^2, \\ \tilde{S}_{a \rightarrow m b c} &\geq \tilde{S}_{a \rightarrow c} + \tilde{S}_{a \rightarrow b} + \tilde{S}_{a \rightarrow m}, \end{aligned} \quad (15)$$

which imply that the quantum resources cannot be freely shared among multipartite systems. In Fig. 5, the entanglement and quantum steering distributions are plotted along with the increasing of the relative coupling g_c/ω_b at the characteristic time τ , where the value of $\tilde{E}_{ac}^2(\tau)$ [$\tilde{S}_{a \rightarrow c}(\tau)$] closely approximates that of $\tilde{E}_{a|m b c}^2(\tau)$ [$\tilde{S}_{a \rightarrow m b c}(\tau)$] and the values of other two-mode resources are negligibly small. The case for the EOM system is similar (see Sec. IV in the SM [65]). This result indicates that multipartite quantum resources in hybrid systems can be optimally squeezed into the MO subsystem under the effective Hamiltonian. Moreover, for the multi-intermediate hybrid system (such as the magneto-optomechanical system [40] with $N = 3$), the effective Hamiltonian method remains valid, while it should be noted that there is a trade-off between more tunable parameters and more physical constraints.

In conclusion, we have developed a general theory of stable MO quantum resources in multipartite hybrid-system dynamics by constructing the effective Hamiltonian. The analytical expressions of stable MO entanglement and quantum steer-

ings are derived for both the steady-state and unsteady-state evolutions, which enable precise quantum control by tuning the effective coupling strength and facilitate multi-parameter optimization on quantum resource generation. Remarkably, our analytical results indicate that the stable MO quantum resources in the unsteady-state evolution exhibit the enhanced quality over the limit of those in the steady-state case. Furthermore, the validity of this analytical approach is confirmed by numerical verification via the full system dynamics for the EOM and COMM hybrid systems. Our work provides not only an analytical theory for the generation of stable MO quantum resources in multipartite MO hybrid systems but also an effective theoretical tool for the future MO converters and distributed quantum networks.

Acknowledgments.—This work was supported by NSFC (Grants No. 12404405, No. 12404330, and No. 11575051), the Guangdong Provincial Quantum Science Strategic Initiative (Grant No. GDZX2404001), Hebei NSF (Grant No. A2021205020 and No. A2025205030), Hebei 333 Talent Project (No. B20231005), and the funds of Hebei Normal University (Grants No. L2024B10 and No. L2026J02).

Data availability.—The data underlying the findings reported in this Letter are not publicly available. The data are available from the authors upon reasonable request.

* qishifan@hebtu.edu.cn

† zwang@hku.hk

‡ ykbai@semi.ac.cn

- [1] M. Aspelmeyer, T. J. Kippenberg, and F. Marquardt, *Cavity optomechanics*, *Rev. Mod. Phys.* **86**, 1391 (2014).
- [2] X. Gu, A. F. Kockum, A. Miranowicz, Y. xi Liu, and F. Nori, *Microwave photonics with superconducting quantum circuits*, *Phys. Rep.* **718-719**, 1 (2017).
- [3] J. Yao, *Microwave Photonics*, *J. Lightwave Technol.* **27**, 314 (2009).
- [4] D. Marpaung, J. Yao, and J. Capmany, *Integrated microwave photonics*, *Nat. Photonics* **13**, 80 (2019).
- [5] S. Barzanjeh, A. Xuereb, S. Gröblacher, M. Paternostro, C. A. Regal, and E. M. Weig, *Optomechanics for quantum technologies*, *Nat. Phys.* **18**, 15 (2022).
- [6] J. Liu, D. Liu, Z. Jin, Z. Lin, H. Li, L. You, X. Feng, F. Liu, K. Cui, W. Zhang, and Y. Huang, *Reconfigurable entanglement distribution network based on pump management of a spontaneous four-wave mixing source*, *Sci. Adv.* **10**, eado9822 (2024).
- [7] Y. Zhang, X. Ding, Y. Li, L. Zhang, Y.-P. Guo, G.-Q. Wang, Z. Ning, M.-C. Xu, R.-Z. Liu, J.-Y. Zhao, G.-Y. Zou, H. Wang, Y. Cao, Y.-M. He, C.-Z. Peng, Y.-H. Huo, S.-K. Liao, C.-Y. Lu, F. Xu, and J.-W. Pan, *Experimental Single-Photon Quantum Key Distribution Surpassing the Fundamental Weak Coherent-State Rate Limit*, *Phys. Rev. Lett.* **134**, 210801 (2025).
- [8] Z.-L. Xiang, S. Ashhab, J. Q. You, and F. Nori, *Hybrid quantum circuits: Superconducting circuits interacting with other quantum systems*, *Rev. Mod. Phys.* **85**, 623 (2013).
- [9] X. Zhang, C.-L. Zou, L. Jiang, and H. X. Tang, *Strongly Coupled Magnons and Cavity Microwave Photons*, *Phys. Rev. Lett.* **113**, 156401 (2014).
- [10] J. L. O’Brien, A. Furusawa, and J. Vučković, *Photonic quan-*

tum technologies, *Nat. Photonics* **3**, 687 (2009).

[11] Y. Lei, F. K. Asadi, T. Zhong, A. Kuzmich, C. Simon, and M. Hosseini, *Quantum optical memory for entanglement distribution*, *Optica* **10**, 1511 (2023).

[12] X. Han, W. Fu, C.-L. Zou, L. Jiang, and H. X. Tang, *Microwave-optical quantum frequency conversion*, *Optica* **8**, 1050 (2021).

[13] N. J. Lambert, A. Rueda, F. Sedlmeir, and H. G. L. Schwefel, *Coherent Conversion Between Microwave and Optical Photons—An Overview of Physical Implementations*, *Adv. Quantum Technol.* **3**, 1900077 (2020).

[14] J. Capmany and D. Novak, *Microwave photonics combines two worlds*, *Nat. Photonics* **1**, 319 (2007).

[15] R. W. Andrews, R. W. Peterson, T. P. Purdy, K. Cicak, R. W. Simmonds, C. A. Regal, and K. W. Lehnert, *Bidirectional and efficient conversion between microwave and optical light*, *Nat. Phys.* **10**, 321 (2014).

[16] M. Forsch, R. Stockill, A. Wallucks, I. Marinković, C. Gärtner, R. A. Norte, F. van Otten, A. Fiore, K. Srinivasan, and S. Gröblacher, *Microwave-to-optics conversion using a mechanical oscillator in its quantum ground state*, *Nat. Phys.* **16**, 69 (2020).

[17] W. Jiang, C. J. Sarabalis, Y. D. Dahmani, R. N. Patel, F. M. Mayor, T. P. McKenna, R. Van Laer, and A. H. Safavi-Naeini, *Efficient bidirectional piezo-optomechanical transduction between microwave and optical frequency*, *Nat. Commun.* **11**, 1166 (2020).

[18] H.-T. Tu, K.-Y. Liao, Z.-X. Zhang, X.-H. Liu, S.-Y. Zheng, S.-Z. Yang, X.-D. Zhang, H. Yan, and S.-L. Zhu, *High-efficiency coherent microwave-to-optics conversion via off-resonant scattering*, *Nat. Photonics* **16**, 291 (2022).

[19] S. Borówka, U. Pylypenko, M. Mazelanik, and M. Paraniak, *Continuous wideband microwave-to-optical converter based on room-temperature Rydberg atoms*, *Nat. Photonics* **18**, 32 (2024).

[20] H. J. Kimble, *The quantum internet*, *Nature (London)* **453**, 1023 (2008).

[21] S. Wehner, D. Elkouss, and R. Hanson, *Quantum internet: A vision for the road ahead*, *Science* **362**, eaam9288 (2018).

[22] N. Gisin and R. Thew, *Quantum communication*, *Nat. Photonics* **1**, 165 (2007).

[23] S. Krastanov, H. Raniwala, J. Holzgrafe, K. Jacobs, M. Lončar, M. J. Reagor, and D. R. Englund, *Optically Heralded Entanglement of Superconducting Systems in Quantum Networks*, *Phys. Rev. Lett.* **127**, 040503 (2021).

[24] R. Horodecki, P. Horodecki, M. Horodecki, and K. Horodecki, *Quantum entanglement*, *Rev. Mod. Phys.* **81**, 865 (2009).

[25] R. Uola, A. C. S. Costa, H. C. Nguyen, and O. Gühne, *Quantum steering*, *Rev. Mod. Phys.* **92**, 015001 (2020).

[26] S. Barzanjeh, M. Abdi, G. J. Milburn, P. Tombesi, and D. Vitali, *Reversible Optical-to-Microwave Quantum Interface*, *Phys. Rev. Lett.* **109**, 130503 (2012).

[27] C. Zhong, Z. Wang, C. Zou, M. Zhang, X. Han, W. Fu, M. Xu, S. Shankar, M. H. Devoret, H. X. Tang, and L. Jiang, *Proposal for Heralded Generation and Detection of Entangled Microwave–Optical-Photon Pairs*, *Phys. Rev. Lett.* **124**, 010511 (2020).

[28] A. Rueda, W. Hease, S. Barzanjeh, and J. M. Fink, *Electro-optic entanglement source for microwave to telecom quantum state transfer*, *npj Quantum Inf.* **5**, 108 (2019).

[29] R. Sahu, L. Qiu, W. Hease, G. Arnold, Y. Minoguchi, P. Rabl, and J. M. Fink, *Entangling microwaves with light*, *Science* **380**, 718 (2023).

[30] J. Bochmann, A. Vainsencher, D. D. Awschalom, and A. N. Cleland, *Nanomechanical coupling between microwave and optical photons*, *Nat. Phys.* **9**, 712 (2013).

[31] S. Barzanjeh, S. Guha, C. Weedbrook, D. Vitali, J. H. Shapiro, and S. Pirandola, *Microwave Quantum Illumination*, *Phys. Rev. Lett.* **114**, 080503 (2015).

[32] S. Barzanjeh, D. Vitali, P. Tombesi, and G. J. Milburn, *Entangling optical and microwave cavity modes by means of a nanomechanical resonator*, *Phys. Rev. A* **84**, 042342 (2011).

[33] H. Tan, X. Zhang, and G. Li, *Steady-state one-way Einstein-Podolsky-Rosen steering in optomechanical interfaces*, *Phys. Rev. A* **91**, 032121 (2015).

[34] C. Zhong, X. Han, H. X. Tang, and L. Jiang, *Entanglement of microwave-optical modes in a strongly coupled electro-optomechanical system*, *Phys. Rev. A* **101**, 032345 (2020).

[35] C. Zhong, X. Han, and L. Jiang, *Microwave and Optical Entanglement for Quantum Transduction with Electro-Optomechanics*, *Phys. Rev. Appl.* **18**, 054061 (2022).

[36] Z.-Y. Fan, L. Qiu, S. Gröblacher, and J. Li, *Microwave-Optics Entanglement Via Cavity Optomagnomechanics*, *Laser Photonics Rev.* **17**, 2200866 (2023).

[37] Y.-X. Luo, L.-J. Cong, Z.-G. Zheng, H.-Y. Liu, Y. Ming, and R.-C. Yang, *Entanglement enhancement and EPR steering based on a PT-symmetric-like cavity-opto-magnomechanical hybrid system*, *Opt. Express* **31**, 34764 (2023).

[38] X. Zhang, C.-L. Zou, L. Jiang, and H. X. Tang, *Cavity magnomechanics*, *Sci. Adv.* **2**, e1501286 (2016).

[39] D. Vitali, S. Gigan, A. Ferreira, H. R. Böhm, P. Tombesi, A. Guerreiro, V. Vedral, A. Zeilinger, and M. Aspelmeyer, *Optomechanical Entanglement between a Movable Mirror and a Cavity Field*, *Phys. Rev. Lett.* **98**, 030405 (2007).

[40] Z. Shen, G.-T. Xu, M. Zhang, Y.-L. Zhang, Y. Wang, C.-Z. Chai, C.-L. Zou, G.-C. Guo, and C.-H. Dong, *Coherent Coupling between Phonons, Magnons, and Photons*, *Phys. Rev. Lett.* **129**, 243601 (2022).

[41] H.-T. Li, Z.-Y. Fan, H.-B. Zhu, S. Gröblacher, and J. Li, *Microwave-Optics Entanglement via Coupled Opto- and Magnomechanical Microspheres*, *Laser Photonics Rev.* **19**, 2401348 (2025).

[42] V. Coffman, J. Kundu, and W. K. Wootters, *Distributed entanglement*, *Phys. Rev. A* **61**, 052306 (2000).

[43] T. J. Osborne and F. Verstraete, *General Monogamy Inequality for Bipartite Qubit Entanglement*, *Phys. Rev. Lett.* **96**, 220503 (2006).

[44] Y.-C. Ou and H. Fan, *Monogamy inequality in terms of negativity for three-qubit states*, *Phys. Rev. A* **75**, 062308 (2007).

[45] Y.-K. Bai, Y.-F. Xu, and Z. D. Wang, *General Monogamy Relation for the Entanglement of Formation in Multiqubit Systems*, *Phys. Rev. Lett.* **113**, 100503 (2014).

[46] G. Adesso, A. Serafini, and F. Illuminati, *Multipartite entanglement in three-mode Gaussian states of continuous-variable systems: Quantification, sharing structure, and decoherence*, *Phys. Rev. A* **73**, 032345 (2006).

[47] T. Hiroshima, G. Adesso, and F. Illuminati, *Monogamy Inequality for Distributed Gaussian Entanglement*, *Phys. Rev. Lett.* **98**, 050503 (2007).

[48] L. Lami, C. Hirche, G. Adesso, and A. Winter, *Schur Complement Inequalities for Covariance Matrices and Monogamy of Quantum Correlations*, *Phys. Rev. Lett.* **117**, 220502 (2016).

[49] X. Deng, Y. Xiang, C. Tian, G. Adesso, Q. He, Q. Gong, X. Su, C. Xie, and K. Peng, *Demonstration of Monogamy Relations for Einstein-Podolsky-Rosen Steering in Gaussian Cluster States*, *Phys. Rev. Lett.* **118**, 230501 (2017).

[50] T. Yu and J. H. Eberly, *Finite-Time Disentanglement Via Spontaneous Emission*, *Phys. Rev. Lett.* **93**, 140404 (2004).

[51] T. Yu and J. H. Eberly, *Sudden Death of Entanglement*, *Science* **323**, 598 (2009).

[52] A. Mari and J. Eisert, *Gently Modulating Optomechanical Systems*, *Phys. Rev. Lett.* **103**, 213603 (2009).

[53] G. Wang, L. Huang, Y.-C. Lai, and C. Grebogi, *Nonlinear Dynamics and Quantum Entanglement in Optomechanical Systems*, *Phys. Rev. Lett.* **112**, 110406 (2014).

[54] S. Chakraborty and A. K. Sarma, *Entanglement dynamics of two coupled mechanical oscillators in modulated optomechanics*, *Phys. Rev. A* **97**, 022336 (2018).

[55] S.-X. Wu, C.-H. Bai, G. Li, C.-s. Yu, and T. Zhang, *Quantum squeezing-induced quantum entanglement and EPR steering in a coupled optomechanical system*, *Opt. Express* **32**, 260 (2024).

[56] J. Maziero, L. C. Céleri, R. M. Serra, and V. Vedral, *Classical and quantum correlations under decoherence*, *Phys. Rev. A* **80**, 044102 (2009).

[57] J.-S. Xu, X.-Y. Xu, C.-F. Li, C.-J. Zhang, X.-B. Zou, and G.-C. Guo, *Experimental investigation of classical and quantum correlations under decoherence*, *Nat. Commun.* **1**, 7 (2010).

[58] L. Mazzola, J. Piilo, and S. Maniscalco, *Sudden Transition between Classical and Quantum Decoherence*, *Phys. Rev. Lett.* **104**, 200401 (2010).

[59] C. Zhu, C. Genes, and B. Stiller, *Optoacoustic Entanglement in a Continuous Brillouin-Active Solid State System*, *Phys. Rev. Lett.* **133**, 203602 (2024).

[60] M. Combescot, *On the generalized golden rule for transition probabilities*, *J. Phys. A: Math. Gen.* **34**, 6087 (2001).

[61] L. Garziano, V. Macrì, R. Stassi, O. Di Stefano, F. Nori, and S. Savasta, *One Photon Can Simultaneously Excite Two or More Atoms*, *Phys. Rev. Lett.* **117**, 043601 (2016).

[62] V. Macrì, F. Nori, and A. F. Kockum, *Simple preparation of Bell and Greenberger-Horne-Zeilinger states using ultrastrong-coupling circuit QED*, *Phys. Rev. A* **98**, 062327 (2018).

[63] S.-f. Qi and J. Jing, *Kerr-magnon-assisted asymptotic stationary photon-phonon squeezing*, *Phys. Rev. A* **111**, 013708 (2025).

[64] C. W. Gardiner and M. J. Collett, *Input and output in damped quantum systems: Quantum stochastic differential equations and the master equation*, *Phys. Rev. A* **31**, 3761 (1985).

[65] See the Supplemental Material for detailed derivations of the main results.

[66] G. Vidal and R. F. Werner, *Computable measure of entanglement*, *Phys. Rev. A* **65**, 032314 (2002).

[67] A. Serafini, F. Illuminati, M. G. A. Paris, and S. De Siena, *Entanglement and purity of two-mode Gaussian states in noisy channels*, *Phys. Rev. A* **69**, 022318 (2004).

[68] G. Adesso, A. Serafini, and F. Illuminati, *Quantification and Scaling of Multipartite Entanglement in Continuous Variable Systems*, *Phys. Rev. Lett.* **93**, 220504 (2004).

[69] G. Adesso and F. Illuminati, *Entanglement in continuous-variable systems: recent advances and current perspectives*, *J. Phys. A: Math. Theor.* **40**, 7821 (2007).

[70] T. Gehring, V. Händchen, J. Duhme, F. Furrer, T. Franz, C. Pacher, and R. Werner, Reinhard F. and Schnabel, *Implementation of continuous-variable quantum key distribution with composable and one-sided-device-independent security against coherent attacks*, *Nat. Commun.* **6**, 8795 (2015).

[71] N. Walk, S. Hosseini, J. Geng, O. Thearle, J. Y. Haw, S. Armstrong, S. M. Assad, J. Janousek, T. C. Ralph, T. Symul, H. M. Wiseman, and P. K. Lam, *Experimental demonstration of Gaussian protocols for one-sided device-independent quantum key distribution*, *Optica* **3**, 634 (2016).

[72] Y. Xiang, S. Cheng, Q. Gong, Z. Ficek, and Q. He, *Quantum Steering: Practical Challenges and Future Directions*, *PRX Quantum* **3**, 030102 (2022).

[73] D. G. Marangon, G. Vallone, and P. Villoresi, *Source-Device-Independent Ultrafast Quantum Random Number Generation*, *Phys. Rev. Lett.* **118**, 060503 (2017).

[74] J. Zhang, Y. Li, M. Zhao, D. Han, J. Liu, M. Wang, Q. Gong, Y. Xiang, Q. He, and X. Su, *One-sided device-independent random number generation through fiber channels*, *Light Sci. Appl.* **14**, 25 (2025).

[75] I. Kogias, A. R. Lee, S. Ragy, and G. Adesso, *Quantification of Gaussian Quantum Steering*, *Phys. Rev. Lett.* **114**, 060403 (2015).

End Matter

The effective Hamiltonian method.—In the main text, we present a general theoretical framework that transforms the chain-type Hamiltonian in Eq. (1) into the effective Hamiltonian H_{eff} in Eq. (2). Here, we give a rigorous derivation for the Hamiltonian H_{eff} as well as the analytical expressions of the effective coupling strength g_{eff} for an arbitrarily given number of intermediate modes.

According to the perturbation theory [61], in the large-detuning regime, $g_a, g_s, g_c \ll \{|\Delta_a - \omega_s|, |\Delta_c - \omega_s|\}$, the Hamiltonian H_0 in Eq. (1) can be treated as the unperturbed term, while the interaction term V is regarded as a perturbation. When the detuning of the microwave mode is approximately opposite to that of the optical mode, namely $\Delta_a \approx -\Delta_c$, the energy differences between certain nondegenerate quantum states of the unperturbed Hamiltonian H_0 can be comparable to, or even smaller than, the strength of the perturbation V . Such states, although formally nondegenerate, can therefore be regarded as nearly degenerate. Under these conditions, the linear interaction described by V can ef-

fectively couple the nearly degenerate states, resulting in an effective Hamiltonian defined within the reduced Hilbert subspace spanned by them.

Specifically, consider two near-degenerate eigenstates $|i\rangle \equiv |n\rangle_a |l_1\rangle_{b_1} \cdots |l_N\rangle_{b_N} |k\rangle_c$ and $|j\rangle \equiv |(n+1)\rangle_a |l_1\rangle_{b_1} \cdots |l_N\rangle_{b_N} |(k+1)\rangle_c$ of the free Hamiltonian H_0 , which can be effectively coupled via the perturbation term V . The effective Hamiltonian within the subspace spanned by $\{|i\rangle, |j\rangle\}$ can be formally written as

$$H_{\text{eff}} = \epsilon_i |i\rangle\langle i| + (\Delta_a + \Delta_c + \epsilon_j) |j\rangle\langle j| + \tilde{g}_{\text{eff}} (|i\rangle\langle j| + |j\rangle\langle i|). \quad (\text{A1})$$

Here, ϵ_i and ϵ_j represent the energy shifts caused by the coupling for states $|i\rangle$ and $|j\rangle$, respectively, and \tilde{g}_{eff} is the effective coupling strength between two target states resulting from the interaction term V . These are the three coefficients to be determined in this ansatz. Note that we here omitted [63] the common unperturbed eigenenergies of the two bases $n\Delta_a + \sum_{s=1}^N l_s \omega_s + k\Delta_c$.

We first consider the effective coupling \tilde{g}_{eff} . According to the standard perturbation theory [61], the effective coupling strength between these two states arising from an N -th order perturbed process can be expressed as

$$\tilde{g}_{\text{eff}} = \sum_{m_1 m_2 \dots m_N} \frac{V_{j m_N} \dots V_{m_2 m_1} V_{m_1 i}}{(E_i - E_{m_N}) \dots (E_i - E_{m_1})} \quad (\text{A2})$$

where $V_{m_{k+1} m_k} \equiv \langle m_{k+1} | V | m_k \rangle$ and $|m_k\rangle$ denotes an eigenstate of H_0 with eigenenergy E_{m_k} . Under the condition that the perturbation strength is much smaller than that of the unperturbed term, i.e., $V_{m_{k+1} m_k} \ll |E_{m_{k+1}} - E_{m_k}|$, the effective coupling strength at N -th order is significantly larger than that at $(N+1)$ -th order. Consequently, in specific derivations, the indirect coupling between the eigenstates $|i\rangle$ and $|j\rangle$ is dominated by the leading-order contributions, and the higher-order effects, such as the third-order corrections are neglected when the second-order effects are already included.

From the definition of \tilde{g}_{eff} in Eq. (A2) and the linear-coupling Hamiltonian in Eq. (1), the effective coupling strength between two target states $|i\rangle$ and $|j\rangle$ is obtained by summing the leading-order contributions from all paths shown in Fig. 6, yielding

$$\tilde{g}_{\text{eff}} = \sqrt{(n+1)(k+1)} g_{\text{eff}}, \quad (\text{A3})$$

where the parameter g_{eff} is given by

$$g_{\text{eff}} = \begin{cases} g_a g_c \left(\frac{\cos \theta \sin \phi}{\Delta_a - \omega_1} - \frac{\sin \theta \cos \phi}{\Delta_a + \omega_1} \right), & N = 1 \\ g_a g_1 g_c \left(\prod_{s=2}^{N-1} \frac{2g_s \omega_s}{\Delta_a^2 - \omega_s^2} \right) \left(\frac{\sin \theta}{\Delta_a + \omega_1} - \frac{\cos \theta}{\Delta_a - \omega_1} \right) \\ \times \left(\frac{\cos \phi}{\Delta_a + \omega_N} - \frac{\sin \phi}{\Delta_a - \omega_N} \right), & N \geq 2 \end{cases} \quad (\text{A4})$$

where the coupling strengths g_a , g_s and g_c , the detuning Δ_a , the transition frequencies ω_1 , ω_s , and ω_N , as well as the angles θ and ϕ follow from Eq. (1). When $s = 2$, the value of $\prod_{s=2}^{N-1} [2g_s \omega_s / (\Delta_a^2 - \omega_s^2)] = 1$. The discrepancy between the cases $N = 1$ and $N \geq 2$ is attributed to the line-type structure of the Hamiltonian in Eq. (1). The effective coupling strength \tilde{g}_{eff} is proportional to $\sqrt{(n+1)(k+1)}$ and independent of the excitation numbers of intermediate modes.

Then, we consider the energy shifts of the eigenstates $|i\rangle$ and $|j\rangle$, given by

$$\epsilon_i = \sum_m \frac{|V_{mi}|^2}{E_i - E_m}, \quad \epsilon_j = \sum_m \frac{|V_{jm}|^2}{E_j - E_m}. \quad (\text{A5})$$

These results are obtained by summing over all virtual paths from $|i\rangle \rightarrow |i\rangle$ ($|j\rangle \rightarrow |j\rangle$) through intermediate states, corresponding to second-order perturbation processes, as shown in Fig. 6. The resulting energy shifts depend only on the target modes and their nearest neighboring modes, and are independent of other intermediate states.

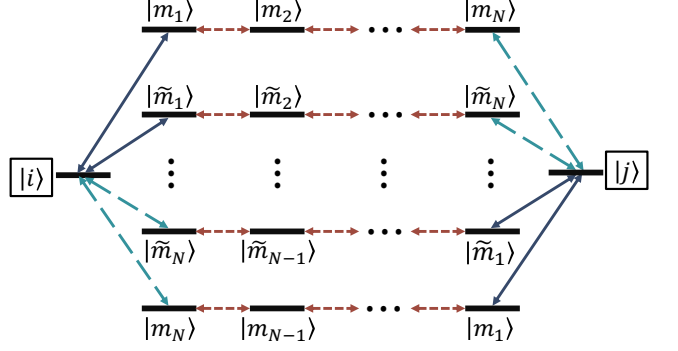


FIG. 6. All leading-order paths connecting $|i\rangle$ and $|j\rangle$ are illustrated. Here, the target states are $|i\rangle \equiv |n\rangle_a |l_1\rangle_{b_1} \dots |l_N\rangle_{b_N} |k\rangle_c$ and $|j\rangle \equiv |(n+1)\rangle_a |l_1\rangle_{b_1} \dots |l_N\rangle_{b_N} |(k+1)\rangle_c$, and the intermediate states are $|m_1\rangle = |(n+1)(l_1+1)l_2 \dots l_N k\rangle$, $|m_2\rangle = |(n+1)l_1(l_2+1) \dots l_N k\rangle$, $|m_N\rangle = |(n+1)l_1 l_2 \dots (l_N+1)k\rangle$, $|\tilde{m}_1\rangle = |(n+1)(l_1-1)l_2 \dots l_N k\rangle$, $|\tilde{m}_2\rangle = |(n+1)l_1(l_2-1) \dots l_N k\rangle$, and $|\tilde{m}_N\rangle = |(n+1)l_1 l_2 \dots (l_N-1)k\rangle$. The solid lines represent the coupling between the microwave mode a and the intermediary mode b_1 , the dashed lines indicate the coupling between the optical mode c and the intermediary mode b_N , and the dotted lines denote the coupling between intermediary modes s and $s+1$ ($s = 1, 2, \dots, N$).

When the condition $\epsilon_i = \Delta_a + \Delta_c + \epsilon_j$ is satisfied, the diagonal terms in the first line of Eq. (A1) form the identity operator within the considered subspace. Defining the difference $\delta \equiv \epsilon_i - \epsilon_j$, we obtain

$$\delta = \frac{g_a^2 [\omega_1 + \Delta_a \cos(2\theta)]}{\omega_1^2 - \Delta_a^2} + \frac{g_c^2 [\omega_N + \Delta_c \cos(2\phi)]}{\omega_N^2 - \Delta_c^2}, \quad (\text{A6})$$

which is independent of particular choice of the near-degenerate states.

Under this condition, i.e., $\Delta_a = -\Delta_c + \delta$, the effective Hamiltonian in Eq. (A1) can be further reduced to

$$\begin{aligned} H_{\text{eff}} &= \tilde{g}_{\text{eff}} (|i\rangle\langle j| + |j\rangle\langle i|) \\ &= \tilde{g}_{\text{eff}} (|nk\rangle\langle (n+1)(k+1)| + \text{h.c.}) \\ &\quad \otimes |l_1 l_2 \dots l_N\rangle\langle l_1 l_2 \dots l_N|. \end{aligned} \quad (\text{A7})$$

Then, by eliminating the decoupled intermediate modes and according to the definition given in Eq. (A3), the effective Hamiltonian is reduced to

$$\begin{aligned} H_{\text{eff}} &= \sqrt{(n+1)(k+1)} g_{\text{eff}} \\ &\quad \times [|nk\rangle\langle (n+1)(k+1)| + \text{h.c.}]. \end{aligned} \quad (\text{A8})$$

Since this result holds for arbitrary n and k , and the bosonic operators satisfy $a^\dagger |n\rangle = \sqrt{n+1} |n+1\rangle$ and $c^\dagger |k\rangle = \sqrt{k+1} |k+1\rangle$, the Hamiltonian in Eq. (A8) defined in the subspace can be straightforwardly extended to the full Hilbert space of modes a and c . Therefore, we eventually obtain

$$H_{\text{eff}} = g_{\text{eff}} (a^\dagger c^\dagger + ac), \quad (\text{A9})$$

where the analytical expression of g_{eff} has the form given in Eq. (A4). The parameter g_{eff} denotes the effective coupling

strength between microwave and optical modes, which depends on the coupling strengths, detunings, and transition frequencies of the intermediate modes. For the fixed $\{\Delta_a, \omega_s\}$, g_{eff} is enhanced with increasing original coupling strengths. Furthermore, it is noted that a larger number of intermediate modes provides greater flexibility for parameter engineering while imposes more physical constraints on the realization of the effective Hamiltonian. In summary, Eq. (A9) together with Eq. (A4) provide an explicit analytical formula for the effective Hamiltonian in the main text.

Moreover, this general theoretical framework can be applied to typical multipartite hybrid quantum systems including the EOM and COMM systems investigated in this work, to derive the effective coupling strengths given in Eqs. (12) and (14). Once the system parameters are given, the effective coupling strength g_{eff} between the two target modes can be directly obtained from Eq. (A4). The explicit constructions of the effective Hamiltonians for the EOM and COMM systems, together with the corresponding path diagrams, are provided in Secs. II A and III A of the SM [65], respectively.

Supplemental Material for “General Theory of Stable Microwave-Optical Quantum Resources in Hybrid-System Dynamics”

Fan Li,¹ Shi-fan Qi,^{1,*} Z. D. Wang,^{2,3,†} and Yan-Kui Bai^{1,3,‡}

¹*College of Physics and Hebei Key Laboratory of Photophysics Research and Application,
Hebei Normal University, Shijiazhuang, Hebei 050024, China*

²*HK Institute of Quantum Science & Technology and Department of Physics,
The University of Hong Kong, Pokfulam Road, Hong Kong, China*

³*Hong Kong Branch for Quantum Science Center of Guangdong-Hong Kong-Macau Greater Bay Area, Shenzhen 518045, China*

CONTENTS

I. System dynamics and quantum resources under the effective Hamiltonian	2
A. Analytical solution for the covariance matrix	2
B. Microwave-optical entanglement	3
C. Microwave-optical quantum steering	3
D. The characteristic time and its verification	5
II. Application in electro-optomechanical systems	6
A. Model and the effective Hamiltonian	6
B. System dynamics and quantum resources	7
III. Application in cavity optomechanical systems	8
A. Model and the effective Hamiltonian	8
B. System dynamics and quantum resources	10
IV. Multipartite entanglement and steering	11
References	12

I. SYSTEM DYNAMICS AND QUANTUM RESOURCES UNDER THE EFFECTIVE HAMILTONIAN

In this section, we investigate the system dynamics within the open-quantum-system framework governed by the effective Hamiltonian in Eq. (2) of the main text, and analyze the generation of stable entanglement and quantum steering between the target modes a and c .

A. Analytical solution for the covariance matrix

Based on the effective Hamiltonian in Eq. (2) of the main manuscript, the dynamics of the quantum system under Markovian environments can be described as the following quantum Langevin equations (QLEs),

$$\begin{aligned}\dot{a} &= -ig_{\text{eff}}c^\dagger - \kappa_a a + \sqrt{2\kappa_a}a_{in}, \\ \dot{c} &= -ig_{\text{eff}}a^\dagger - \kappa_c c + \sqrt{2\kappa_c}c_{in},\end{aligned}\quad (\text{S1})$$

where g_{eff} denotes the effective coupling strength, which is non-zero. κ_a and κ_c represent the decay rates of the modes a and c , respectively. a_{in} and c_{in} are Gaussian noise operators and characterized by their covariance functions, $\langle o_{in}(t)o_{in}^\dagger(t') \rangle = [N_o + 1]\delta(t - t')$ and $\langle o_{in}^\dagger(t)o_{in}(t') \rangle = N_o\delta(t - t')$ ($o = a, c$), where $N_o = [\exp(\hbar\omega_o/k_B T) - 1]^{-1}$ is the mean population number of mode o at the thermal equilibrium state, k_B is the Boltzmann constant and T is the environmental temperature.

The QLEs in Eq. (S1) can be written in a matrix form of

$$\dot{u}(t) = A_{\text{eff}}u(t) + \xi_{\text{eff}}(t), \quad (\text{S2})$$

where $u(t) = [X_a(t), Y_a(t), X_c(t), Y_c(t)]^T$ and $X_o = (o + o^\dagger)/\sqrt{2}$, $Y_o = (o - o^\dagger)/i\sqrt{2}$ ($o = a, c$). The drift matrix A_{eff} is given by

$$A_{\text{eff}} = -\begin{pmatrix} \kappa_a & 0 & 0 & g_{\text{eff}} \\ 0 & \kappa_a & g_{\text{eff}} & 0 \\ 0 & g_{\text{eff}} & \kappa_c & 0 \\ g_{\text{eff}} & 0 & 0 & \kappa_c \end{pmatrix}. \quad (\text{S3})$$

$\xi_{\text{eff}}(t) = [\sqrt{2\kappa_a}X_a^{in}, \sqrt{2\kappa_a}Y_a^{in}, \sqrt{2\kappa_c}X_c^{in}, \sqrt{2\kappa_c}Y_c^{in}]^T$ is the vector of Gaussian noise operators and $X_o^{in} = (o_{in} + o_{in}^\dagger)/\sqrt{2}$, $Y_o^{in} = (o_{in} - o_{in}^\dagger)/i\sqrt{2}$.

Given that the quantum state is a Gaussian state, the system dynamics can be fully characterized by a 4×4 covariance matrix (CM). With the QLE in Eq. (S2), the dynamics of the CM $v(t)$ satisfies

$$\dot{v}(t) = A_{\text{eff}}v(t) + v(t)A_{\text{eff}}^T + D_{\text{eff}}. \quad (\text{S4})$$

The elements of $v(t)$ are defined as $v_{ij}(t) = \langle u_i(t)u_j(t) + u_j(t)u_i(t) \rangle / 2 - \langle u_i(t) \rangle \langle u_j(t) \rangle$ ($i, j = 1, 2, 3, 4$), where $u_i(t)$ is the i -term of $u(t)$ in Eq. (S2). $D_{\text{eff}} = \text{diag}[\kappa_a(2N_a + 1), \kappa_a(2N_a + 1), \kappa_c(2N_c + 1), \kappa_c(2N_c + 1)]$ is the diffusion matrix and defined by $D_{\text{eff}}_{ij}\delta(t - t') = \langle \xi_{\text{eff}}_i(t)\xi_{\text{eff}}_j(t') \rangle / 2$. In this situation, we consider the hybrid system in an ultra-low-temperature environment and accordingly set $N_a = N_c = 0$ in the following contents.

At the initial time, two target modes are assumed in the vacuum states, i.e., the CM satisfies $v(0) = I_4/2$, where I_4 is an identity matrix with four dimensions. Under this condition, the non-zero matrix elements in $v(t)$ can be analytically derived as

$$\begin{aligned}v_{11}(t) &= (1 + \sin \varphi)c_-e^{-(\Omega + \kappa_a + \kappa_c)t} - c_0e^{-(\kappa_a + \kappa_c)t} \\ &\quad + (1 - \sin \varphi)c_+e^{(\Omega - \kappa_a - \kappa_c)t} + c_1, \\ v_{44}(t) &= (1 - \sin \varphi)c_-e^{-(\Omega + \kappa_a + \kappa_c)t} + c_0e^{-(\kappa_a + \kappa_c)t} \\ &\quad + (1 + \sin \varphi)c_+e^{(\Omega - \kappa_a - \kappa_c)t} + c_2, \\ v_{14}(t) &= \cos \varphi c_-e^{-(\Omega + \kappa_a + \kappa_c)t} + c_0 \tan \varphi e^{-(\kappa_a + \kappa_c)t} \\ &\quad - \cos \varphi c_+e^{(\Omega - \kappa_a - \kappa_c)t} + c_3,\end{aligned}\quad (\text{S5})$$

and $v_{22}(t) = v_{11}(t)$, $v_{33}(t) = v_{44}(t)$, $v_{23}(t) = v_{14}(t)$. The parameters are defined as

$$\begin{aligned}\Omega &= \sqrt{4g_{\text{eff}}^2 + (\kappa_a - \kappa_c)^2}, \quad \tan \varphi = \frac{\kappa_a - \kappa_c}{2g_{\text{eff}}}, \\ c_\pm &= \frac{\Omega - (\kappa_a - \kappa_c)\sin \varphi}{4[\Omega \mp (\kappa_a + \kappa_c)]}, \quad c_0 = \frac{\cos^2 \varphi(\kappa_a - \kappa_c)}{2(\kappa_a + \kappa_c)}.\end{aligned}\quad (\text{S6})$$

The constants c_1 , c_2 , and c_3 are

$$\begin{aligned}c_1 &= \frac{1}{2} - \frac{g_{\text{eff}}}{\kappa_a}c_3, \quad c_2 = \frac{1}{2} - \frac{g_{\text{eff}}}{\kappa_c}c_3, \\ c_3 &= \frac{g_{\text{eff}}\kappa_a\kappa_c}{(\kappa_a + \kappa_c)(g_{\text{eff}}^2 - \kappa_a\kappa_c)}.\end{aligned}\quad (\text{S7})$$

The steady-state regime requires the CM elements to be invariant values, i.e., $\dot{v}(t) = 0$. Under this condition, the elements are $v_{11} = c_1$, $v_{44} = c_2$ and $v_{14} = c_3$. Through the definitions in Eq. (S7), a legitimate CM requires $g_{\text{eff}}^2 < \kappa_a\kappa_c$. In the steady-state regime, one can easily demonstrate that the exponent factor $\Omega - \kappa_a - \kappa_c < 0$ in Eq. (S5) via the definition Ω in Eq. (S6). That leads to $v_{11}(\infty) = c_1$, $v_{44}(\infty) = c_2$, and $v_{14}(\infty) = c_3$. These elements under steady states are the asymptotic values as $t \rightarrow \infty$. Conversely, when $g_{\text{eff}}^2 > \kappa_a\kappa_c$, the CM elements are exponentially divergent due to the exponent factor $\Omega - \kappa_a - \kappa_c > 0$, yielding the system's CM dynamics is unsteady. At the critical point, $g_{\text{eff}}^2 = \kappa_a\kappa_c$, the exponent factor satisfies $\Omega - \kappa_a - \kappa_c = 0$, and the system's CM exhibits an approximately linear divergence in this case. Accordingly, the system dynamics can be classified into two distinct regimes, the steady-state regime characterized by

$$g_{\text{eff}}^2 < \kappa_a\kappa_c \quad (\text{S8})$$

and the unsteady-state regime corresponding to

$$g_{\text{eff}}^2 \geq \kappa_a\kappa_c. \quad (\text{S9})$$

B. Microwave-optical entanglement

We now analyze the bipartite entanglement between the microwave mode a and the optical mode c , based on the sys-

tem dynamics presented in Sec. IA. The resulting microwave-optical (MO) entanglement is quantified via the logarithmic negativity (LN) [1], which is defined as

$$E_{ac}(t) = \max[0, -\ln(2\eta_{ac}^-)], \quad (\text{S10})$$

where $\eta_{ac}^- = [\Gamma - (\Gamma^2 - 4 \det v)^{1/2}]^{1/2}/\sqrt{2}$ is the minimum symplectic eigenvalue of the partial transpose of the CM $v(t) = [v_a, v_{ac}; v_{ac}^T, v_c]$, with v_a , v_c , and v_{ac} denoting the 2×2 subblocks of $v(t)$, and $\Gamma \equiv \det v_a + \det v_c - 2 \det v_{ac}$. By the definition in Eq. (S10) and CM shown in Eq. (S5), we can obtain the time-dependent MO entanglement criterion

$$\begin{aligned} E_{ac}(t) &= -\ln[\zeta_{ac}(t)], \\ \zeta_{ac}(t) &= (v_{11} + v_{44})(1 - \sqrt{1 + x}), \\ x &= \frac{4(v_{14}^2 - v_{11}v_{44})}{(v_{11} + v_{44})^2}. \end{aligned} \quad (\text{S11})$$

For simplicity, we denote $v_{11} = v_{11}(t)$, $v_{44} = v_{44}(t)$ and $v_{14} = v_{14}(t)$. By combining the CM elements shown in Eq. (S5) with the properties of the CM, one can demonstrate that $0 < \zeta_{ac} < 1$.

In the steady-state regime, $g_{\text{eff}}^2 < \kappa_a \kappa_c$, all of the CM elements given in Eq. (S7) approach steady values when $t \rightarrow \infty$, i.e., $v_{11}(\infty) = c_1$, $v_{44}(\infty) = c_2$, and $v_{14}(\infty) = c_3$. By substituting the values of c_1 , c_2 and c_3 in Eq. (S7) into Eq. (S11), the stable LN at $t \rightarrow \infty$ can be derived as

$$E_{ac}(\infty) = -\ln[\zeta_{ac}(\infty)] = \ln\left(\frac{\kappa_a \kappa_c - g_{\text{eff}}^2}{\kappa_a \kappa_c - g_{\text{eff}}^2 \chi}\right), \quad (\text{S12})$$

where $\chi = \{1 + 4\kappa_a \kappa_c(\kappa_a \kappa_c - g_{\text{eff}}^2)/[g_{\text{eff}}^2(\kappa_a + \kappa_c)^2]\}^{1/2}$. For simplicity and with no loss of generality, we apply the convention $E_{ac}(\infty) \rightarrow E_{ac}$ and $\zeta_{ac}(\infty) \rightarrow \zeta_{ac}$ in the main manuscript and following content.

Next, we examine the MO entanglement generation beyond the steady-state regime, i.e., for $g_{\text{eff}}^2 \geq \kappa_a \kappa_c$. In this unsteady-state regime, via the CM elements in Eq. (S5), one can demonstrate that the parameter x given in Eq. (S11) approaches zero in the long-time limit, i.e., $x \rightarrow 0$ as $t \rightarrow \infty$. This allows a first-order expansion of ζ_{ac} in x using the Taylor expansion $\sqrt{1 + x} \approx 1 + x/2$, yielding $\zeta_{ac} = -(v_{11} + v_{44})x/2$. Consequently, the entanglement E_{ac} in the long-time limit can be obtained as

$$E_{ac} = \ln\left(1 + 4\frac{g_{\text{eff}}^2}{\tilde{\chi}}\right), \quad (\text{S13})$$

where $\tilde{\chi} = \Omega(\kappa_a + \kappa_c) + (\kappa_a - \kappa_c)^2$ and Ω is given in Eq. (S6).

By combining Eqs. (S12) and (S13), one can obtain

$$E_{ac} = \begin{cases} \ln\left(\frac{\kappa_a \kappa_c - g_{\text{eff}}^2}{\kappa_a \kappa_c - g_{\text{eff}}^2 \chi}\right), & g_{\text{eff}}^2 < \kappa_a \kappa_c \\ \ln\left(1 + 4\frac{g_{\text{eff}}^2}{\tilde{\chi}}\right), & g_{\text{eff}}^2 \geq \kappa_a \kappa_c \end{cases} \quad (\text{S14})$$

which is the Eq. (7) given in the main text. It can be concluded that stable MO entanglement can be achieved irrespective of the system's dynamical evolution, both in the steady-state and unsteady-state regimes. Moreover, it should be noted that as $g_{\text{eff}}^2 \rightarrow (\kappa_a \kappa_c)^{-}$, Eq. (S12) approaches the upper bound of steady-state MO entanglement, which coincides with the result of Eq. (S13), i.e.,

$$\lim_{g_{\text{eff}}^2 \rightarrow (\kappa_a \kappa_c)^{-}} E_{ac} = \ln\left[\frac{(\kappa_a + \kappa_c)^2}{\kappa_a^2 + \kappa_c^2}\right]. \quad (\text{S15})$$

Therefore, the piecewise-defined LN E_{ac} given in Eq. (S14) is a continuous function of the independent variable g_{eff}^2 .

Next, we analyze the monotonicity of LN E_{ac} . When $g_{\text{eff}}^2 < \kappa_a \kappa_c$, the dependence of E_{ac} on g_{eff}^2 can be inferred from the analysis of $\partial E_{ac}/\partial g_{\text{eff}}^2$, which can be expressed as

$$\frac{\partial E_{ac}}{\partial g_{\text{eff}}^2} = \frac{\zeta_{ac} \kappa_a \kappa_c [g_{\text{eff}}(\kappa_a + \kappa_c) - \Lambda]^2}{2(\kappa_a \kappa_c - g_{\text{eff}}^2 \chi)^2 (\kappa_a + \kappa_c)^2 g_{\text{eff}}^2 \chi}, \quad (\text{S16})$$

where $\Lambda = [g_{\text{eff}}^2(\kappa_a - \kappa_c)^2 + 4\kappa_a^2 \kappa_c^2]^{1/2}$. One can observe that $\partial E_{ac}/\partial g_{\text{eff}}^2 > 0$ for the value of g_{eff}^2 , indicating that E_{ac} increases monotonically with g_{eff}^2 . In the unsteady-state regime, $\tilde{\chi}$ is positive and scales linearly with Ω [Eq. (S6)]. As a result, the entanglement E_{ac} in Eq. (S13) increases monotonically with g_{eff}^2 . Consequently, the LN E_{ac} defined in Eq. (S14) is a continuous, monotonically increasing function of the independent variable g_{eff}^2 . Therefore, operating in the unsteady-state regime enables the generation of stronger MO entanglement than in the steady-state condition.

C. Microwave-optical quantum steering

Similarly, we analyze the quantum steering between the microwave mode a and the optical mode c based on the system dynamics presented in Sec. IA. The MO quantum steering can be measured by [2]

$$\begin{aligned} S_{a \rightarrow c}(t) &= \max[0, S_{ac}], \\ S_{c \rightarrow a}(t) &= \max[0, S_{ca}], \end{aligned} \quad (\text{S17})$$

where the quantities $S_{ac}(t) = \ln[\det v_a/(4\det v)]/2$ and $S_{ca}(t) = \ln[\det v_c/(4\det v)]/2$. $S_{a \rightarrow c} > 0$ ($S_{c \rightarrow a} > 0$) is proven that the bipartite Gaussian state characterized by the CM can be steered from microwave (optical) mode to optical (microwave) mode. Based on the definition in Eq. (S17) and the CM of Eq. (S5), we derive the time-dependent quantum steering quantities

$$\begin{aligned} S_{ac}(t) &= \ln\left[\frac{v_{11}}{2(v_{14}^2 - v_{11}v_{44})}\right], \\ S_{ca}(t) &= \ln\left[\frac{v_{44}}{2(v_{14}^2 - v_{11}v_{44})}\right]. \end{aligned} \quad (\text{S18})$$

In the steady-state regime ($g_{\text{eff}}^2 < \kappa_a \kappa_c$), the values of S_{ac}

and S_{ca} can be derived as

$$\begin{aligned} S_{ac}(\infty) &= \ln \left[\frac{g_{\text{eff}}^2(\kappa_c^2 - \kappa_a^2) + \Xi}{g_{\text{eff}}^2(\kappa_a - \kappa_c)^2 + \Xi} \right], \\ S_{ca}(\infty) &= \ln \left[\frac{g_{\text{eff}}^2(\kappa_a^2 - \kappa_c^2) + \Xi}{g_{\text{eff}}^2(\kappa_a - \kappa_c)^2 + \Xi} \right], \end{aligned} \quad (\text{S19})$$

where $\Xi = \kappa_a \kappa_c (\kappa_a + \kappa_c)^2$. For simplicity, we apply the convention $S_{ac}(\infty) \rightarrow S_{ac}$ and $S_{ca}(\infty) \rightarrow S_{ca}$ in the following content and main text.

Moreover, by substituting the CM elements in Eq. (S5) into Eq. (S18), the quantities S_{ac} and S_{ca} in the unsteady-state regime ($g_{\text{eff}}^2 \geq \kappa_a \kappa_c$) can be derived. In the long-time limit $t \rightarrow \infty$, they are given by

$$\begin{aligned} S_{ac} &= \ln \left(\frac{\Omega - \kappa_a + \kappa_c}{2\Omega} \right) + E_{ac}, \\ S_{ca} &= \ln \left(\frac{\Omega + \kappa_a - \kappa_c}{2\Omega} \right) + E_{ac}, \end{aligned} \quad (\text{S20})$$

where E_{ac} is shown in Eq. (S13).

By combining Eqs. (S19) and (S20), the quantity S_{ac} can be expressed as

$$S_{ac} = \begin{cases} \ln \left[\frac{g_{\text{eff}}^2(\kappa_c^2 - \kappa_a^2) + \Xi}{g_{\text{eff}}^2(\kappa_a - \kappa_c)^2 + \Xi} \right], & g_{\text{eff}}^2 < \kappa_a \kappa_c \\ \ln \left(\frac{\Omega - \kappa_a + \kappa_c}{2\Omega} \right) + E_{ac}, & g_{\text{eff}}^2 \geq \kappa_a \kappa_c \end{cases} \quad (\text{S21})$$

which corresponds to Eq. (9) in the main text. The steering value S_{ca} is obtained by interchanging κ_a and κ_c in Eq. (S21). Furthermore, when $g_{\text{eff}}^2 \rightarrow (\kappa_a \kappa_c)^-$, S_{ac} and S_{ca} respectively reach their maximum values under the steady-state regime. These results correspond to the values of S_{ac} and S_{ca} in Eq. (S20), i.e.,

$$\begin{aligned} \lim_{g_{\text{eff}}^2 \rightarrow (\kappa_a \kappa_c)^-} S_{ac} &= \ln \left[\frac{\kappa_a \kappa_c + \kappa_c^2}{\kappa_a^2 + \kappa_c^2} \right], \\ \lim_{g_{\text{eff}}^2 \rightarrow (\kappa_a \kappa_c)^-} S_{ca} &= \ln \left[\frac{\kappa_a^2 + \kappa_a \kappa_c}{\kappa_a^2 + \kappa_c^2} \right]. \end{aligned} \quad (\text{S22})$$

Both quantities are continuous functions of g_{eff}^2 .

Next, we identify the parameter regimes for realizing quantum steering by analyzing Eq. (S21). In the steady-state regime, for $\kappa_a < \kappa_c$, one finds $S_{ac} > 0$ and $S_{ca} < 0$, indicating that the bipartite entangled state is steerable from mode a to mode c , whereas steering from c to a is forbidden. Conversely, when $\kappa_a > \kappa_c$, $S_{ca} > 0$ while $S_{ac} < 0$, implying that mode c can steer mode a . The special case $\kappa_a = \kappa_c$ corresponds to a critical point at which quantum steering vanishes in both directions, i.e., $S_{ac} = S_{ca} = 0$. Accordingly, the parameter ranges required to realize one-way steering in the steady-state regime are given by

$$\begin{aligned} S_{a \rightarrow c} : \kappa_a < \kappa_c, 0 < g_{\text{eff}}^2 < \kappa_a \kappa_c, \\ S_{c \rightarrow a} : \kappa_a > \kappa_c, 0 < g_{\text{eff}}^2 < \kappa_a \kappa_c. \end{aligned} \quad (\text{S23})$$

Similarly, the parameter ranges required to realize stable quantum steering in the unsteady-state regime can be derived as

$$\begin{aligned} S_{a \rightarrow c} &\begin{cases} \kappa_a \leq \kappa_c, & g_{\text{eff}}^2 > \kappa_a \kappa_c \\ \kappa_a > \kappa_c, & g_{\text{eff}}^2 > \kappa_a (2\kappa_a - \kappa_c) \end{cases}, \\ S_{c \rightarrow a} &\begin{cases} \kappa_a < \kappa_c, & g_{\text{eff}}^2 > \kappa_c (2\kappa_c - \kappa_a) \\ \kappa_a \geq \kappa_c, & g_{\text{eff}}^2 > \kappa_a \kappa_c \end{cases}. \end{aligned} \quad (\text{S24})$$

Notably, two-way quantum steering between modes a and c emerges when the coupling strength g_{eff} is increased such that $g_{\text{eff}}^2 + \kappa_a \kappa_c > 2\kappa_a^2, 2\kappa_c^2$.

Then, we analyze the monotonicity of the steering quantities. In the steady-state regime, the monotonic behavior of the steering quantities can be demonstrated by analyzing the derivatives $\partial S_{ac}/\partial g_{\text{eff}}^2$ and $\partial S_{ca}/\partial g_{\text{eff}}^2$, which are given by

$$\begin{aligned} \frac{\partial S_{ac}}{\partial g_{\text{eff}}^2} &= \frac{2\kappa_a \Xi (\kappa_c - \kappa_a)}{[\Xi + (\kappa_a - \kappa_c)]^2}, \\ \frac{\partial S_{ca}}{\partial g_{\text{eff}}^2} &= \frac{2\kappa_c \Xi (\kappa_a - \kappa_c)}{[\Xi + (\kappa_a - \kappa_c)]^2}, \end{aligned} \quad (\text{S25})$$

where $\Xi > 0$ is defined in Eq. (S19). Under the condition $S_{ac} > 0$ for $\kappa_a < \kappa_c$, one directly obtains $\partial S_{ac}/\partial g_{\text{eff}}^2 > 0$. Similarly, when $S_{ca} > 0$ for $\kappa_a > \kappa_c$, it follows that $\partial S_{ca}/\partial g_{\text{eff}}^2 > 0$. From the above analysis, it can be concluded that both $S_{a \rightarrow c}$ and $S_{c \rightarrow a}$ increase monotonically with increasing the magnitude of g_{eff} . Moreover, a similar analysis shows that, in the unsteady-state regime, both S_{ac} and S_{ca} increase monotonically with g_{eff}^2 .

Furthermore, we clarify the relation between MO entanglement and quantum steering. In the steady-state regime, we define the ratios $\mathcal{R}_{ac} \equiv E_{ac}/S_{ac}$ and $\mathcal{R}_{ca} \equiv E_{ac}/S_{ca}$, which can be derived as

$$\begin{aligned} \mathcal{R}_{ac} &= 1 + \frac{\sqrt{4\kappa_a^2 \kappa_c^2 g_{\text{eff}}^2 + \mathcal{K}_{ac}^2} - \mathcal{K}_{ac}}{\kappa_a \kappa_c (\kappa_a + \kappa_c) + \mathcal{K}_{ac}}, \\ \mathcal{R}_{ca} &= 1 + \frac{\sqrt{4\kappa_a^2 \kappa_c^2 g_{\text{eff}}^2 + \mathcal{K}_{ca}^2} - \mathcal{K}_{ca}}{\kappa_a \kappa_c (\kappa_a + \kappa_c) + \mathcal{K}_{ca}}, \end{aligned} \quad (\text{S26})$$

where $\mathcal{K}_{ac} = g_{\text{eff}}^2(\kappa_c - \kappa_a)$ and $\mathcal{K}_{ca} = g_{\text{eff}}^2(\kappa_a - \kappa_c)$. Under the condition $\kappa_a < \kappa_c$, one has $S_{ac} > 0$ and $\mathcal{K}_{ac} > 0$, leading to a ratio $\mathcal{R}_{ac} > 1$. Similarly, for $\kappa_a > \kappa_c$, $S_{ca} > 0$ and $\mathcal{K}_{ca} > 0$, yielding $\mathcal{R}_{ca} > 1$. These results provide an analytical demonstration that, in the steady-state regime, quantum steering constitutes a strict subset of MO entanglement. In the unsteady-state regime, according to the definition of Ω in Eq. (S6), $\Omega - \kappa_a + \kappa_c < 2\Omega$ and $\Omega + \kappa_a - \kappa_c < 2\Omega$. Consequently, the first logarithmic terms in Eqs. (S20) are negative, implying $S_{ac}, S_{ca} < E_{ac}$. This shows that quantum steering is still strictly bounded by the corresponding MO entanglement in the unsteady-state condition.

In the open-quantum-system framework, the effective two-mode squeezing interaction and the environmental noises constitute a competitive mechanism. Over time, the two-mode

squeezing interaction generates and gradually increases the quantum entanglement and steering. In contrast, the decoherence noises progressively degrade the MO entanglement and quantum steering. That results in the entanglement E_{ac} and steering $S_{a \rightarrow c}$ and $S_{c \rightarrow a}$ approaching stability progressively.

D. The characteristic time and its verification

In practical numerical simulations, the evolution time cannot be taken to infinity. Therefore, a sufficiently long time τ must be chosen to faithfully approximate the asymptotic long-time limit. We now turn to the determination of this characteristic time τ . Under the transformation

$$X = \sin \frac{\varphi}{2} X_a + \cos \frac{\varphi}{2} Y_c, \quad Y = \cos \frac{\varphi}{2} X_a - \sin \frac{\varphi}{2} Y_c, \quad (\text{S27})$$

ζ_{ac} in Eq. (S11) turns into

$$\zeta_{ac} = \Delta X + \Delta Y - \sqrt{(\Delta X - \Delta Y)^2 + 4 \langle XY \rangle^2}. \quad (\text{S28})$$

Using the CM elements given in Eq. (S5), the variance $\Delta X = \langle X^2 \rangle - \langle X \rangle^2$ can be expressed as

$$\Delta X(t) = \frac{1}{2} + 2c_- e^{-(\Omega + \kappa_a + \kappa_c)t} - 2c_-, \quad (\text{S29})$$

the variance $\Delta Y = \langle Y^2 \rangle - \langle Y \rangle^2$ is

$$\Delta Y(t) = \frac{1}{2} + 2c_+ e^{(\Omega - \kappa_a - \kappa_c)t} - 2c_+, \quad (\text{S30})$$

and the correlation term $\langle X(t)Y(t) \rangle$ is obtained as

$$\langle X(t)Y(t) \rangle = \frac{c_0}{\cos \varphi} \left[1 + e^{-(\kappa_a + \kappa_c)t} \right]. \quad (\text{S31})$$

The definitions of c_{\pm} , c_0 , φ , and Ω are given in Eq. (S6).

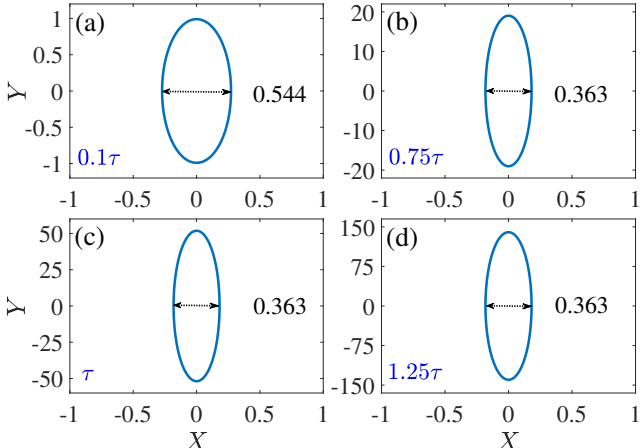


FIG. S1. Quantum fluctuations in the X and Y quadratures at different evolution times, 0.1τ , 0.75τ , τ , and 1.25τ . We set $g_{\text{eff}}^2/\kappa_a \kappa_c = 4$ and $\kappa_c = 2\kappa_a$ are fixed for all panels.

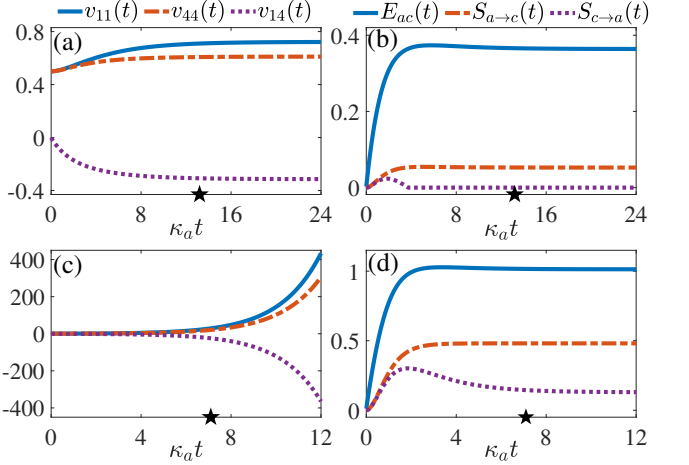


FIG. S2. Numerical verification of theoretical results. [(a), (c)] The dynamical evolution of the CM elements $v_{11}(t)$, $v_{44}(t)$, and $v_{14}(t)$ under steady-state and unsteady-state conditions, respectively. [(b), (d)] Time evolution of the entanglement E_{ac} , steering $S_{a \rightarrow c}$ and $S_{c \rightarrow a}$ under steady-state and unsteady-state conditions, respectively. For (a) and (b), $g_{\text{eff}}^2/\kappa_a \kappa_c = 0.5$, and for (c) and (d), $g_{\text{eff}}^2/\kappa_a \kappa_c = 4$. $\kappa_c = 2\kappa_a$ is fixed for all panels. The star symbols mark the point corresponding to the characteristic time τ .

In the unsteady-state regime, the exponential term in Eq. (S30) is positive, i.e., $\Omega - \kappa_a - \kappa_c > 0$. Consequently, after sufficiently long evolution, one finds $\Delta Y(t) \gg \Delta X(t)$, $\langle X(t)Y(t) \rangle$. Under this condition, $\zeta_{ac}(t)$ can be approximated as

$$\zeta_{ac}(t) \approx 2\Delta X(t) = 1 + 4c_- e^{-(\Omega + \kappa_a + \kappa_c)t} - 4c_-. \quad (\text{S32})$$

We can then define a characteristic time

$$\tau = \frac{4\pi}{\Omega + \kappa_a + \kappa_c}, \quad (\text{S33})$$

which approximately represents the timescale for the system to establish stable quantum resources. At $t = \tau$, $e^{-4\pi} \ll 1$ (numerically $\sim 10^{-6}$), so that $\zeta_{ac}(\tau) \approx 2\Delta X(\tau) \approx 2\Delta X(\infty) \approx \zeta_{ac}(\infty)$. From Eq. (S29), it follows that increasing $|g_{\text{eff}}|$ reduces τ , enabling faster stabilization of the quantum resources. Moreover, for the steady-state case, the long-time limit (as $t \rightarrow \infty$) is obtained by setting $\dot{v} = 0$ in Eq. (S4). Therefore, we define the characteristic time primarily for the unsteady-state regime.

In Fig. S1, we investigate the evolution of quantum fluctuations of the generalized quadrature operator $\hat{O} = \cos \psi X + \sin \psi Y$, where $\psi \in [0, 2\pi]$. In this plot, the ellipse's minor axis along x represents ΔX , while the major axis along y represents ΔY . Over time, ΔY increases rapidly, whereas ΔX grows briefly before saturating at 0.363, already stabilized by the characteristic time τ .

Our theoretical results from the preceding Secs. IA-ID can be numerically verified through the CM elements and quantum resources, as illustrated in Fig. S2. In Fig. S2(a), the CM elements $v_{11}(t)$, $v_{44}(t)$, and $v_{14}(t)$ approach stable values after extended evolution, reflecting the steady-state regime. In

contrast, Fig. S2(c) shows these elements diverging exponentially over time, indicating unsteady system dynamics. Unlike the CM elements, which exhibit distinctly different behavior under steady-state and unsteady-state conditions, quantum entanglement and steering display consistent dynamical features, tending toward stability over time. The results are shown in Figs. S2(b) and (d), corresponding to the CM results in Figs. S2(a) and (c), respectively. In both regimes, the MO entanglement $E_{ac}(t)$ and steering $S_{a \rightarrow c}(t)$ rise rapidly at early times and become stable before the characteristic time τ , while $S_{c \rightarrow a}(t)$ initially grows and then decays toward its asymptotic value. Notably, the values of $E_{ac}(t)$, $S_{a \rightarrow c}(t)$, and $S_{c \rightarrow a}(t)$ in Fig. S2(d) are larger than the corresponding values in Fig. S2(b). Furthermore, Fig. S2(d) clearly shows two-way steering, with $S_{a \rightarrow c}(t) > S_{c \rightarrow a}(t) > 0$. These observations indicate that the unsteady-state regime can exhibit stronger quantum resources.

II. APPLICATION IN ELECTRO-OPTOMECHANICAL SYSTEMS

A. Model and the effective Hamiltonian

A hybrid electro-optomechanical (EOM) system is considered for generating MO quantum resources. As shown in Fig. S3, the system consists of a microwave LC resonator, a mechanical oscillator, and an optical cavity, which has been realized in recent works [3, 4]. The mechanical oscillator is capacitively coupled to the microwave resonator on one side, while on the other side, it is coupled to the optical cavity via the radiation pressure. A microwave driving field and an optical laser are simultaneously applied to the microwave resonator and optical cavity, respectively. In the rotating frame with respect to the driving frequencies, the Hamiltonian of the EOM system [3, 4] is ($\hbar \equiv 1$)

$$H_{S_1} = \Delta_a a^\dagger a + \omega_b b^\dagger b + \Delta_c c^\dagger c + g_{ab} a^\dagger a (b + b^\dagger) + g_{bc} c^\dagger c (b + b^\dagger) + i\Omega_a (a^\dagger - a) + i\Omega_c (c^\dagger - c), \quad (\text{S34})$$

where a (a^\dagger), b (b^\dagger), and c (c^\dagger) are the annihilation (creation) operators of the microwave, mechanical, and optical modes,

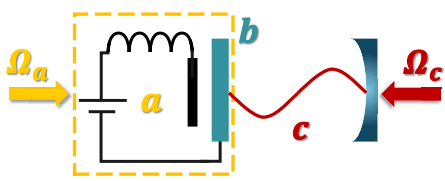


FIG. S3. Schematic of the electro-optomechanical system. The mechanical oscillator acts as an intermediate mode b , coupling with the microwave resonator a and optical cavity c . The microwave and optical modes are driven by a microwave drive field Ω_a and an optical driving laser Ω_c , respectively.

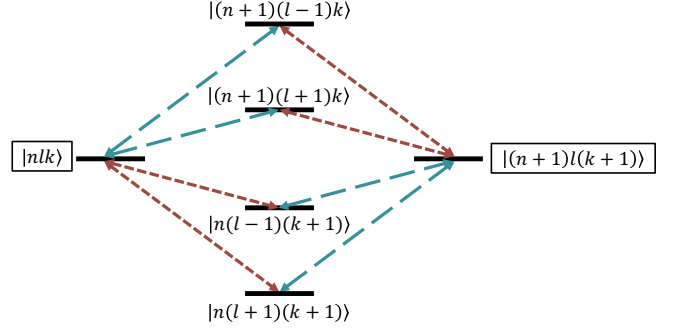


FIG. S4. All four second-order paths connecting $|nlk\rangle$ and $|(n+1)l(k+1)\rangle$ are depicted. The dashed lines represent the coupling between the microwave and mechanical modes, while the dotted lines indicate the coupling between the optical and mechanical modes.

respectively. $\Delta_o = \omega_o - \epsilon_o$ ($o = a, c$) denotes the detuning of mode o , where ω_o is the transition frequency and ϵ_o is the corresponding driving-field frequency. ω_b is the transition frequency of the mechanical mode. The coupling strengths g_{ab} and g_{bc} describe the microwave-mechanical and optomechanical interactions, respectively, which can be enhanced by strongly driving the microwave and optical modes with Rabi frequencies Ω_a and Ω_c .

The microwave and optical modes under strong driving are assumed to have large expectation amplitudes $|\langle a \rangle| \gg 1$ and $|\langle c \rangle| \gg 1$. This allows us to linearize the system dynamics by writing the operators $o = \delta o + \langle o \rangle$, with δo describing the fluctuation of the mode o . Neglecting the second-order fluctuation terms [3, 4], the Hamiltonian in Eq. (S34) becomes

$$H_{S_1} = H_0 + V, \quad H_0 = \sum_{o=a,c} \Delta_o \delta o^\dagger \delta o + \omega_b b^\dagger b, \quad (\text{S35})$$

$$V = \sum_{o=a,c} g_o (\delta o + \delta o^\dagger) (b + b^\dagger),$$

where $g_a = g_{ab} \langle a \rangle$ and $g_c = g_{bc} \langle c \rangle$ are the enhanced microwave-mechanical and optomechanical coupling strength, respectively. For simplicity and without loss of generality, we assume that the values $\langle o \rangle$ are real numbers and make $\delta o \rightarrow o$ in the following content. The linearized Hamiltonian in Eq. (S35) is obtained by setting $\theta = \phi = \pi/4$ and $N = 1$ in the general Hamiltonian in the main text, along with the substitutions $\omega_1 \rightarrow \omega_b$, $b_1 \rightarrow b$, and $g_o \rightarrow \sqrt{2}g_o$. Then, we can use the general effective Hamiltonian construction approach presented in the End Matter to derive the effective coupling of the MO subsystem in the specific EOM system.

Specifically, when the microwave detuning Δ_a is nearly opposite to the optical detuning Δ_c , and both of them are far resonant from mechanical frequency ω_b , i.e., $\Delta_a + \Delta_c \approx 0$ and $g_a, g_c \ll \{|\Delta_a - \omega_b|, |\Delta_c - \omega_b|\}$, the tensor product state $|nlk\rangle \equiv |n\rangle_a |l\rangle_b |k\rangle_c$ approximately degenerates with $|n+1\rangle_l |k+1\rangle_c$. Here, the subscripts a , b , and c represent the microwave, mechanical, and optical modes, respectively, and n , l , and k denote the corresponding Fock states. Under these

cases, the interaction term V in Eq. (S35) can effectively couple the arbitrary base pairs $|nlk\rangle$ and $|(n+1)l(k+1)\rangle$, yielding an effective Hamiltonian expressed in the following form

$$H_{\text{eff}} = \epsilon_1 |nlk\rangle\langle nlk| + (\Delta_a + \Delta_c + \epsilon_2) \times |(n+1)l(k+1)\rangle\langle(n+1)l(k+1)| + \tilde{g}_{\text{eff}} (|nlk\rangle\langle(n+1)l(k+1)| + \text{h.c.}) \quad (\text{S36})$$

Here, ϵ_1 and ϵ_2 represent the energy shifts caused by the coupling between the states $|nlk\rangle$ and $|(n+1)l(k+1)\rangle$, and \tilde{g}_{eff} is the effective coupling strength. These are three coefficients to be determined. It should be noted that the common unperturbed eigenenergies of the two bases, $n\Delta_a + l\omega_b + k\Delta_c$, have been omitted.

We first consider the effective coupling strength \tilde{g}_{eff} between states $|nlk\rangle$ and $|(n+1)l(k+1)\rangle$. As shown in Fig. S4, we summarize all four paths connecting these states and their corresponding contributions to the effective coupling. According to Eq. (A2) in the End Matter, we obtain

$$\tilde{g}_{\text{eff}} = \frac{2g_a g_c \omega_b}{\Delta_a^2 - \omega_b^2} \sqrt{(n+1)(k+1)} \quad (\text{S37})$$

up to the second-order perturbation of coupling strengths g_a and g_c . Similarly, according to Eq. (A6) in the End Matter, the difference δ can be derived as

$$\delta \equiv \epsilon_1 - \epsilon_2 = \frac{2(g_a^2 + g_c^2)\omega_b}{\omega_b^2 - \Delta_a^2}. \quad (\text{S38})$$

Hence, under the condition $\Delta_a = -\Delta_c + \delta$, the effective Hamiltonian in Eq. (S36) can be expressed as

$$H_{\text{eff}} = \tilde{g}_{\text{eff}} (|nlk\rangle\langle(n+1)l(k+1)| + \text{h.c.}) \equiv g_{\text{eff}} \sqrt{(n+1)(k+1)} (|nlk\rangle\langle(n+1)l(k+1)| + \text{h.c.}) \otimes |l\rangle\langle l|. \quad (\text{S39})$$

By neglecting the mechanical mode, the Hamiltonian in Eq. (S39) can be extended to the full Hilbert space of the microwave and optical modes and ultimately takes the form

$$H_{\text{eff}} = g_{\text{eff}} (a^\dagger c^\dagger + ac), \quad (\text{S40})$$

and the coupling strength can be derived as

$$g_{\text{eff}} = \frac{2\omega_b g_a g_c}{\Delta_a^2 - \omega_b^2}. \quad (\text{S41})$$

This is exactly the effective coupling strength of the EOM system reported in the manuscript.

B. System dynamics and quantum resources

This section is devoted to calculating the CM of the full hybrid EOM system. Within the open-quantum-system framework and under standard Markovian environments, one can

derive the QLEs for the full Hamiltonian in Eq. (S35).

$$\begin{aligned} \dot{a} &= -(i\Delta_a + \kappa_a)a - ig_a(b + b^\dagger) + \sqrt{2\kappa_a}a_{in}, \\ \dot{c} &= -(i\Delta_c + \kappa_c)c - ig_c(b + b^\dagger) + \sqrt{2\kappa_c}c_{in}, \\ \dot{b} &= -(i\omega_b + \kappa_b)b - i \sum_{o=a,c} g_o(o + o^\dagger) + \sqrt{2\kappa_b}b_{in}, \end{aligned} \quad (\text{S42})$$

where κ_o ($o = a, b, c$) are the decay rates of the microwave, mechanical, and optical modes, respectively. The input noise operator o_{in} has zero mean and satisfies the correlation functions, $\langle o_{in}(t)o_{in}^\dagger(t') \rangle = [N_o(\omega_o) + 1]\delta(t - t')$ and $\langle o_{in}^\dagger(t)o_{in}(t') \rangle = N_o(\omega_o)\delta(t - t')$. Here, $N_o(\omega_o) = [\exp(\hbar\omega_o/k_B T) - 1]^{-1}$ is the average thermal excitation number, with the Boltzmann constant k_B and the environmental temperature T .

By introducing the quadrature operators $X_o(t) = (o + o^\dagger)/\sqrt{2}$ and $Y_o(t) = (o - o^\dagger)/i\sqrt{2}$, the above Eq. (S42) can be written in the matrix form

$$\dot{\tilde{u}}(t) = A\tilde{u}(t) + \xi(t) \quad (\text{S43})$$

where $\tilde{u}(t) = [u(t)^T, X_b(t), Y_b(t)]^T$ and $u(t)$ is shown in Eq. (S2). $\xi(t) = [\xi_{\text{eff}}^T(t), \sqrt{2\kappa_b}X_b^{in}(t), \sqrt{2\kappa_b}Y_b^{in}(t)]^T$, $\xi_{\text{eff}}(t)$ is the noise vector in Eq. (S2), $X_b^{in}(t) = (b_{in} + b_{in}^\dagger)/\sqrt{2}$ and $Y_b^{in}(t) = (b_{in} - b_{in}^\dagger)/i\sqrt{2}$ are the quadratures of the input noise operators. The drift matrix A is given by

$$A = \begin{pmatrix} -\kappa_a & \Delta_a & 0 & 0 & 0 & 0 \\ -\Delta_a & -\kappa_a & 0 & 0 & -2g_a & 0 \\ 0 & 0 & -\kappa_c & \Delta_c & 0 & 0 \\ 0 & 0 & -\Delta_c & -\kappa_c & -2g_c & 0 \\ 0 & 0 & 0 & 0 & -\kappa_b & \omega_b \\ -2g_a & 0 & -2g_c & 0 & -\omega_b & -\kappa_b \end{pmatrix}. \quad (\text{S44})$$

Owing to the linear dynamics in Eq. (S43) and Gaussian input noises, the system state remains Gaussian. Accordingly, the EOM system can be fully characterized by the 6×6 CM $\tilde{v}_{ij}(t) = \langle \tilde{u}_i(t)\tilde{u}_j(t) + \tilde{u}_j(t)\tilde{u}_i(t) \rangle / 2 - \langle \tilde{u}_i(t) \rangle \langle \tilde{u}_j(t) \rangle$ ($i, j = 1, 2, \dots, 6$), which satisfies

$$\dot{\tilde{v}}(t) = A\tilde{v}(t) + \tilde{v}(t)A^T + D, \quad (\text{S45})$$

where $D = \text{diag}[\kappa_a(2N_a + 1), \kappa_a(2N_a + 1), \kappa_c(2N_c + 1), \kappa_c(2N_c + 1), \kappa_b(2N_b + 1), \kappa_b(2N_b + 1)]$ is the diffusion matrix and defined by $D_{ij}\delta(t - t') = \langle \xi_i(t)\xi_j(t') + \xi_j(t')\xi_i(t) \rangle / 2$. The CM of the MO subsystem is given by $v = \tilde{v}(1 : 4; 1 : 4)$. The corresponding numerical results for the linearized Hamiltonian in Eq. (S35) can then be obtained by solving the above differential equation.

For the specific EOM system, the main manuscript presents numerical results for various quantum resources under different coupling strengths g_a , demonstrating that these resources can be precisely controlled via g_a . In the following, we provide additional results to elucidate the dependence of quantum resources on other physical parameters, including the coupling strength g_c and the detuning Δ_a .

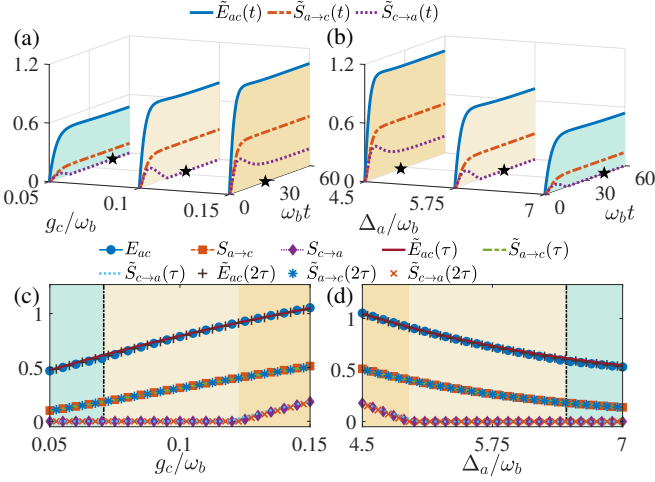


FIG. S5. [(a), (b)] Dynamics of MO quantum resources for different coupling strengths g_c and detunings Δ_a , respectively. Star symbols indicate the values of τ . [(c), (d)] Theoretical predictions (lines of marks) of MO quantum resources, together with numerical results at times τ (lines) and 2τ (marks), shown versus the coupling strength g_c and detuning Δ_a , respectively. The black dot-dashed lines denote the boundary between steady-state (left) and unsteady-state (right) regimes in (c) and (d). E_{ac} , $S_{a\rightarrow c}$, and $S_{c\rightarrow a}$ are evaluated from the theoretical predictions ($t \rightarrow \infty$), while \tilde{E}_{ac} , $\tilde{S}_{a\rightarrow c}$, and $\tilde{S}_{c\rightarrow a}$ are obtained from the full Hamiltonian. $\Delta_a = 5\omega_b$ for (a) and (c). $g_c = 0.12\omega_b$ for (b) and (d). Other parameters are set as $g_a = 0.12\omega_b$, $\kappa_c = 0.5\kappa_a = 10^{-3}\omega_b$, $\kappa_b = 10^{-6}\omega_b$, $N_a = N_c = 0$, and $N_b = 10$.

As shown in Figs. S5(a) and (b), both the MO entanglement \tilde{E}_{ac} and quantum steering $\tilde{S}_{a\rightarrow c}$ initially increase rapidly before stabilizing, whereas $\tilde{S}_{c\rightarrow a}$ exhibits distinct dynamics, rising to a peak before decaying to an asymptotic value. In Fig. S5(a), quantum resources increase with g_c . At $g_c = 0.05\omega_b$, $\tilde{E}_{ac} \approx 0.47$ and $\tilde{S}_{a\rightarrow c} \approx 0.1$ are relatively weak; at $g_c = 0.1\omega_b$, they rise to $\tilde{E}_{ac} \approx 0.79$ and $\tilde{S}_{a\rightarrow c} \approx 0.31$; and further enhancement to $g_c = 0.15\omega_b$ yields asymmetric two-way steering ($\tilde{E}_{ac} \approx 1.05$, $\tilde{S}_{a\rightarrow c} \approx 0.51$, and $\tilde{S}_{c\rightarrow a} \approx 0.17$). By contrast, in Fig. S5(b), the quantum resources decrease with increasing detuning Δ_a . At $\Delta_a = 4.5\omega_b$, asymmetric two-way steering is observed ($\tilde{S}_{a\rightarrow c} > \tilde{S}_{c\rightarrow a} > 0$). Dynamically stable quantum resources can thus be controlled via g_c and Δ_a . A quantitative analysis of the MO entanglement and quantum steering at times τ and 2τ is presented in Figs. S5(c) and (d). The numerical results for \tilde{E}_{ac} , $\tilde{S}_{a\rightarrow c}$, and $\tilde{S}_{c\rightarrow a}$ at time τ and 2τ agree well with the discrete markers representing theoretical predictions from Eqs. (S14) and (S21).

Quantum steering $\tilde{S}_{a\rightarrow c}(\tau)$ and $\tilde{S}_{c\rightarrow a}(\tau)$ are shown in Fig. S6 over the parameter space of microwave and optical decay rates. $\tilde{S}_{a\rightarrow c} > 0$ arises in regions I and II for $\kappa_a < \kappa_c$, while $\tilde{S}_{c\rightarrow a} > 0$ occurs in regions IV and V for $\kappa_a > \kappa_c$, independent of whether the dynamics are steady or unsteady. Quantum steering vanishes in the steady state near $\kappa_a \simeq \kappa_c$, whereas two-way steering emerges ($S_{a\leftrightarrow c} > 0$) in the unsteady-state regime at lower decay rates in region V. Moreover, the smaller the decay rate κ_a , the broader the range

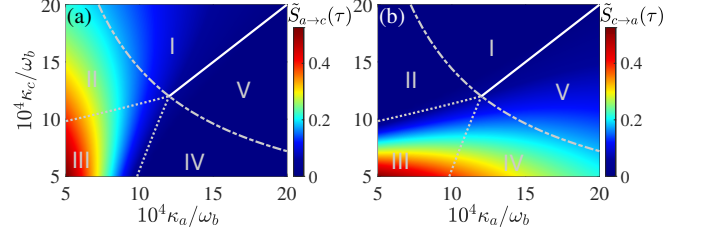


FIG. S6. The performance of quantum steering $\tilde{S}_{a\rightarrow c}(\tau)$ and $\tilde{S}_{c\rightarrow a}(\tau)$ with varying decay rates κ_a and κ_c , respectively. The gray dot-dashed lines delineate the theoretically predicted boundary between the unsteady-state (left) and steady-state (right) regions. The white line marks the theoretically predicted disappearance of quantum steering. The gray dotted line represents the theoretical regime of two-way steering. $g_c = 0.12\omega_b$ and other parameters are the same as Fig. S5.

of κ_c that sustains high-quality $\tilde{S}_{a\rightarrow c}$, and vice versa. For instance, at $\kappa_a = 5 \times 10^{-4}\omega_b$, a wide range $5 \leq 10^4\kappa_c/\omega_b \leq 20$ yields $\tilde{S}_{a\rightarrow c} > 0.2$, as shown in Fig. S6(a). All numerical results are in excellent agreement with the theoretical predictions of Eqs. (S23) and (S24).

The parameters discussed above are feasible in recent experiments [3, 4]. The mechanical frequency is approximately $\omega_b/2\pi \sim 10-100\text{MHz}$, with a decay rate $\kappa_b \sim 10^{-6}\omega_b$ [5, 6]. The decay rates for microwave and optical modes are $\kappa_a, \kappa_c \sim 10^{-5}\omega_b - 10^{-3}\omega_b$ [3, 4]. Under strong driving conditions, the enhanced microwave-mechanical and optomechanical coupling strengths are $g_a, g_c \sim 0.1\omega_b$ [3-5]. It is demonstrated that the cooperativity can exceed unity, $C \equiv g_{\text{eff}}^2/\kappa_a\kappa_c > 1$, thereby realizing the unsteady-state dynamical regime. Besides, both the microwave and optical occupations approach zero, while the mechanical mode $N_b \sim 1-10$ at low temperatures $T \sim 10\text{mK}$ [5].

III. APPLICATION IN CAVITY OPTOMAGNOMECHANICAL SYSTEMS

A. Model and the effective Hamiltonian

To demonstrate the generality of our approach, we further analyze the generation of MO resources in a cavity optomagnomechanical (COMM) system [5], as illustrated in Fig. S7. In the rotating frame with respect to the driving frequencies, the Hamiltonian of the COMM system is ($\hbar \equiv 1$)

$$\begin{aligned} H_{S2} = & \Delta_a a^\dagger a + \Delta_m m^\dagger m + \omega_b b^\dagger b + \Delta_c c^\dagger c \\ & + g_a (a^\dagger m + a m^\dagger) + g_m m^\dagger m (b + b^\dagger) \\ & + g_{bc} c^\dagger c (b + b^\dagger) + i\Omega_a (a^\dagger - a) \\ & + i\Omega_c (c^\dagger - c), \end{aligned} \quad (\text{S46})$$

where a (a^\dagger), m (m^\dagger), b (b^\dagger), and c (c^\dagger) are the annihilation (creation) operators of the microwave, magnon, mechanical, and optical modes. $\Delta_o = \omega_o - \epsilon_o$ ($o = a, m, c$) denotes

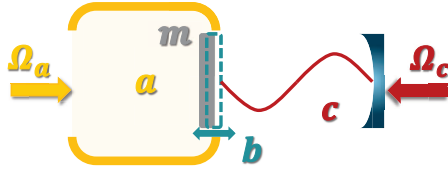


FIG. S7. Schematic of the cavity optomagnomechanical system. A YIG crystal is placed inside a microwave cavity near the maximum magnetic field in microwave mode a , which provides the magnon mode m . It simultaneously serves as a vibrating end mirror (mechanical mode b) of the optical cavity c . The microwave and optical photon modes are driven by a microwave drive field Ω_a and an optical driving laser Ω_c , respectively.

the detuning of mode o , with ω_o and ϵ_o being the transition and driving-field frequencies, respectively, and $\epsilon_m = \epsilon_a$. ω_b is the transition frequency of the mechanical mode. g_a is the microwave-magnon coupling strength, which has entered into the strong coupling regime. The magnomechanical (optomechanical) coupling strength g_{mb} (g_{bc}) is typically small, considering the large frequency mismatch between the magnon (optical) and the mechanical modes, yet it can be significantly enhanced by driving the microwave (optical) mode with a strong field with Rabi frequency Ω_a (Ω_c).

All microwave, magnon, and optical modes have considerable expectation values under strong driving fields. This allows us to linearize [5] the system dynamics by writing the operators $o = \delta o + \langle o \rangle$ ($o = a, m, c$), where $\langle o \rangle$ is the steady-state value and δo represents the quantum fluctuations of the mode o . The Hamiltonian in Eq. (S46) turns to

$$H_{S2} = H_0 + V, \quad H_0 = \omega_b b^\dagger b + \sum_{o=a,m,c} \Delta_o o^\dagger o, \\ V = g_a (a^\dagger m + a m^\dagger) + \sum_{o=m,c} g_o (o + o^\dagger) (b + b^\dagger) \quad (S47)$$

where $g_m = g_{mb} \langle m \rangle$ and $g_c = g_{bc} \langle c \rangle$ are the effective magnomechanical and optomechanical effective coupling strengths, respectively. For simplicity and without loss of generality, we assume $\langle o \rangle$ is a real number and make $\delta o \rightarrow o$ in the following content. It corresponds to the linearized Hamiltonian given in Eq. (1) of the main text for the specific case $\theta = 0$, $\phi = \pi/4$, and $N = 2$, with the substitutions $\omega_1 \rightarrow \Delta_m$, $\omega_2 \rightarrow \omega_b$, $g_c \rightarrow \sqrt{2}g_c$, $b_1 \rightarrow m$, and $b_2 \rightarrow b$. Then, we apply the general effective Hamiltonian construction approach introduced in the End Matter to derive the effective coupling of the MO target subsystem in the COMM system.

When the microwave detuning Δ_a is near opposite the optical detuning Δ_c , and both of them are far resonant from the magnon detuning Δ_m and the mechanical frequency ω_b , i.e., $\Delta_a \approx -\Delta_c$ and $g_a, g_m, g_c \ll \{|\Delta_a - \Delta_m|, |\Delta_c - \omega_b|\}$, it is found that the tensor-product state $|nljk\rangle \equiv |n\rangle_a |l\rangle_m |j\rangle_b |k\rangle_c$ is near-degenerate with $|(n+1)lj(k+1)\rangle$. Using perturbation theory, the effective Hamiltonian for transitions between any base-pair $|nljk\rangle$ and $|(n+1)lj(k+1)\rangle$ can be analytically

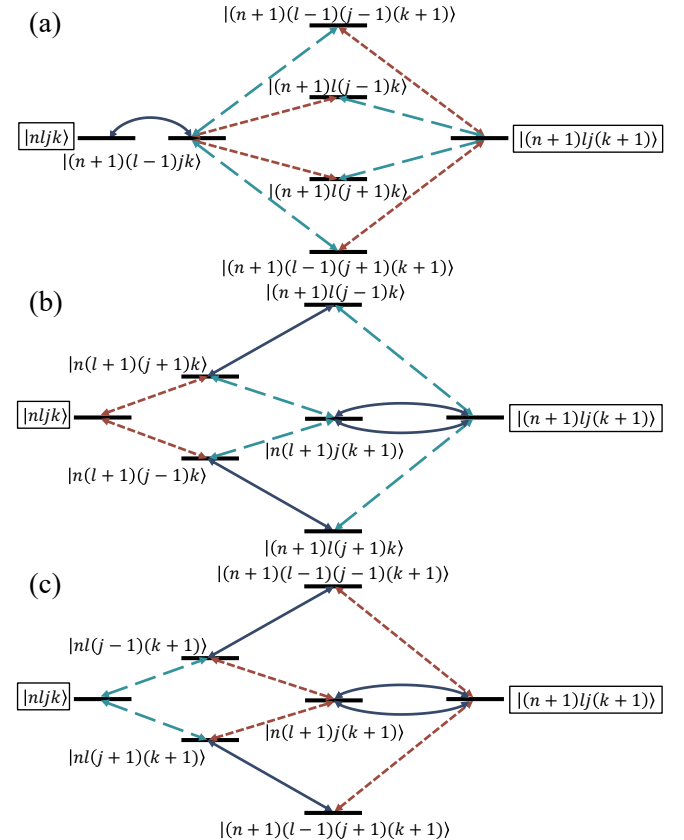


FIG. S8. All twelve third-order (leading order) paths connecting $|nljk\rangle$ and $|(n+1)lj(k+1)\rangle$. Solid, dotted, and dashed lines represent the couplings between the microwave and magnon modes, the magnon and mechanical modes, and the optical and mechanical modes, respectively.

derived. It can be written in the following form

$$H_{\text{eff}} = \epsilon_1 |nljk\rangle \langle nljk| + (\Delta_a + \Delta_c + \epsilon_2) \times |(n+1)lj(k+1)\rangle \langle (n+1)lj(k+1)| \\ + \tilde{g}_{\text{eff}} (|nljk\rangle \langle (n+1)lj(k+1)| + \text{h.c.}), \quad (S48)$$

where ϵ_1 and ϵ_2 are the energy shifts induced by the coupling of the states $|nljk\rangle$ and $|(n+1)lj(k+1)\rangle$, respectively, and \tilde{g}_{eff} is the effective coupling strength. Here, we omit the common unperturbed eigenenergy of two bases.

Using Eq. (A2) in the End Matter and summing over all twelve paths in Fig. S8, we obtain the effective coupling strength

$$\tilde{g}_{\text{eff}} = \frac{2\omega_b g_a g_m g_c}{(\Delta_m - \Delta_a)(\omega_b^2 - \Delta_a^2)} \sqrt{(n+1)(k+1)} \quad (S49)$$

up to the third-order perturbation of coupling strengths. Similarly, via Eq. (A6) in the End Matter, the second-order energy shift δ can be derived as

$$\delta \equiv \epsilon_1 - \epsilon_2 = \frac{g_a^2}{\Delta_m - \Delta_a} + \frac{g_c^2}{\omega_b - \Delta_a} + \frac{g_c^2}{\omega_b + \Delta_a}. \quad (S50)$$

Therefore, under the condition $\Delta_a = -\Delta_c + \delta$, the effective Hamiltonian in Eq. (S48) can be derived as

$$H_{\text{eff}} = \tilde{g}_{\text{eff}} (|nljk\rangle\langle(n+1)lj(k+1)| + \text{h.c.}) \\ \equiv g_{\text{eff}} \sqrt{(n+1)(k+1)} (|nk\rangle\langle(n+1)(k+1)| + \text{h.c.}) \otimes |lj\rangle\langle lj|. \quad (\text{S51})$$

The magnon and mechanical modes can be eliminated. Expanding the effective Hamiltonian in Eq. (S51) in subspace to the full Hilbert space of microwave and optical modes, the effective Hamiltonian in Eq. (S51) eventually becomes

$$H_{\text{eff}} = g_{\text{eff}} (a^\dagger c^\dagger + ac), \quad (\text{S52})$$

and the coupling strength can be written as

$$g_{\text{eff}} = \frac{2g_a g_m g_c \omega_b}{(\Delta_m - \Delta_a)(\omega_b^2 - \Delta_a^2)}. \quad (\text{S53})$$

This is precisely the effective coupling strength in the COMM system given in the manuscript.

B. System dynamics and quantum resources

This section contributes to the calculation of CM for full hybrid COMM system. In the open-quantum-system framework, under the standard Markovian environments, one can arrive at the QLEs for the full linearized Hamiltonian in Eq.

(S47)

$$\dot{a} = -(i\Delta_a + \kappa_a)a - ig_a m + \sqrt{2\kappa_a}a_{in}, \\ \dot{c} = -(i\Delta_c + \kappa_c)c - ig_c(b + b^\dagger) + \sqrt{2\kappa_c}c_{in}, \\ \dot{m} = -(i\Delta_m + \kappa_m)m - ig_a a - ig_m(b + b^\dagger) \\ + \sqrt{2\kappa_m}m_{in}, \quad (\text{S54})$$

$$\dot{b} = -(i\omega_b + \kappa_b)b - i \sum_{o=m,c} g_o(o + o^\dagger) + \sqrt{2\kappa_b}b_{in},$$

where κ_o ($o = a, c, m, b$) are the decay rates of the microwave, optical, magnon, and mechanical modes, respectively. The input noise operator o_{in} is zero mean and satisfies the correlation functions, $\langle o_{in}(t)o_{in}^\dagger(t') \rangle = [N_o(\omega_o) + 1]\delta(t - t')$ and $\langle o_{in}^\dagger(t)o_{in}(t') \rangle = N_o(\omega_o)\delta(t - t')$, where $N_o(\omega_o)$ is the corresponding average thermal excitation number.

By introducing the quadrature operators $X_o(t) = (o + o^\dagger)/\sqrt{2}$ and $Y_o(t) = (o - o^\dagger)/i\sqrt{2}$, the above Eqs. (S54) can be written in the matrix form

$$\dot{\tilde{u}}(t) = A\tilde{u}(t) + \xi(t) \quad (\text{S55})$$

where $\tilde{u}(t) = [u(t)^T, X_m(t), Y_m(t), X_b(t), Y_b(t)]^T$ and $u(t)$ is shown in Eq. (S2). $\xi(t) = [\xi_{\text{eff}}^T(t), \sqrt{2\kappa_m}X_m^{in}(t), \sqrt{2\kappa_m}Y_m^{in}(t), \sqrt{2\kappa_b}X_b^{in}(t), \sqrt{2\kappa_b}Y_b^{in}(t)]^T$, $\xi_{\text{eff}}(t)$ is the noise vector in Eq. (S2), $X_o^{in}(t) = (o_{in} + o_{in}^\dagger)/\sqrt{2}$ and $Y_o^{in}(t) = (o_{in} - o_{in}^\dagger)/i\sqrt{2}$ ($o = m, b$) are the quadratures of the input noise operators. The drift matrix A is given by

$$A = \begin{pmatrix} -\kappa_a & \Delta_a & 0 & 0 & 0 & g_a & 0 & 0 \\ -\Delta_a & -\kappa_a & 0 & 0 & -g_a & 0 & 0 & 0 \\ 0 & 0 & -\kappa_c & \Delta_c & 0 & 0 & 0 & 0 \\ 0 & 0 & -\Delta_c & -\kappa_c & 0 & 0 & -2g_c & 0 \\ 0 & g_a & 0 & 0 & -\kappa_m & \Delta_m & 0 & 0 \\ -g_a & 0 & 0 & 0 & -\Delta_m & -\kappa_m & -2g_m & 0 \\ 0 & 0 & 0 & 0 & 0 & 0 & -\kappa_b & \omega_b \\ 0 & 0 & -2g_c & 0 & -2g_m & 0 & -\omega_b & -\kappa_b \end{pmatrix}. \quad (\text{S56})$$

Using the above linear dynamics described in Eq. (S55), the full system can be characterized by a time-dependent CM, whose elements are defined as $\tilde{v}_{ij}(t, t') = \langle \tilde{u}_i(t)\tilde{u}_j(t') + \tilde{u}_j(t')\tilde{u}_i(t) \rangle / 2 - \langle \tilde{u}_i(t) \rangle \langle \tilde{u}_j(t) \rangle$ ($i, j = 1, 2, \dots, 8$), and which satisfies

$$\dot{\tilde{v}}(t) = A\tilde{v}(t) + \tilde{v}(t)A^T + D, \quad (\text{S57})$$

where $D = \text{diag}[\kappa_a(2N_a + 1), \kappa_a(2N_a + 1), \kappa_c(2N_c + 1), \kappa_c(2N_c + 1), \kappa_m(2N_m + 1), \kappa_m(2N_m + 1), \kappa_b(2N_b + 1), \kappa_b(2N_b + 1)]$ is the diffusion matrix and defined by $D_{ij}\delta(t - t') = \langle \xi_i(t)\xi_j(t') + \xi_j(t')\xi_i(t) \rangle / 2$. The CM of the MO subsystem is $v = \tilde{v}(1 : 4; 1 : 4)$. Then, the numerical results via the full Hamiltonian (S47) can be obtained by

calculating the above differential equation.

In Fig. S9, we present the numerical MO quantum resources at specific times 0.1τ , τ , and 2τ , based on the full system dynamics described by Eq. (S57), along with the corresponding theoretical predictions under identical parameters. At 0.1τ , the values \tilde{E}_{ac} , $\tilde{S}_{a \rightarrow c}$, and $\tilde{S}_{c \rightarrow a}$ remain relatively weak compared to those at τ . By τ , the system develops stable quantum resources, as evidenced by the nearly identical values at τ and 2τ , consistent with theoretical predictions, $\tilde{E}_{ac}(\tau) \approx \tilde{E}_{ac}(2\tau) \approx E_{ac}$, $\tilde{S}_{a \rightarrow c}(\tau) \approx \tilde{S}_{a \rightarrow c}(2\tau) \approx S_{a \rightarrow c}$, and $\tilde{S}_{c \rightarrow a}(\tau) \approx \tilde{S}_{c \rightarrow a}(2\tau) \approx S_{c \rightarrow a}$. This demonstrates that stable MO entanglement and quantum steering are established after a sufficient evolution time $\sim \tau$, in agreement

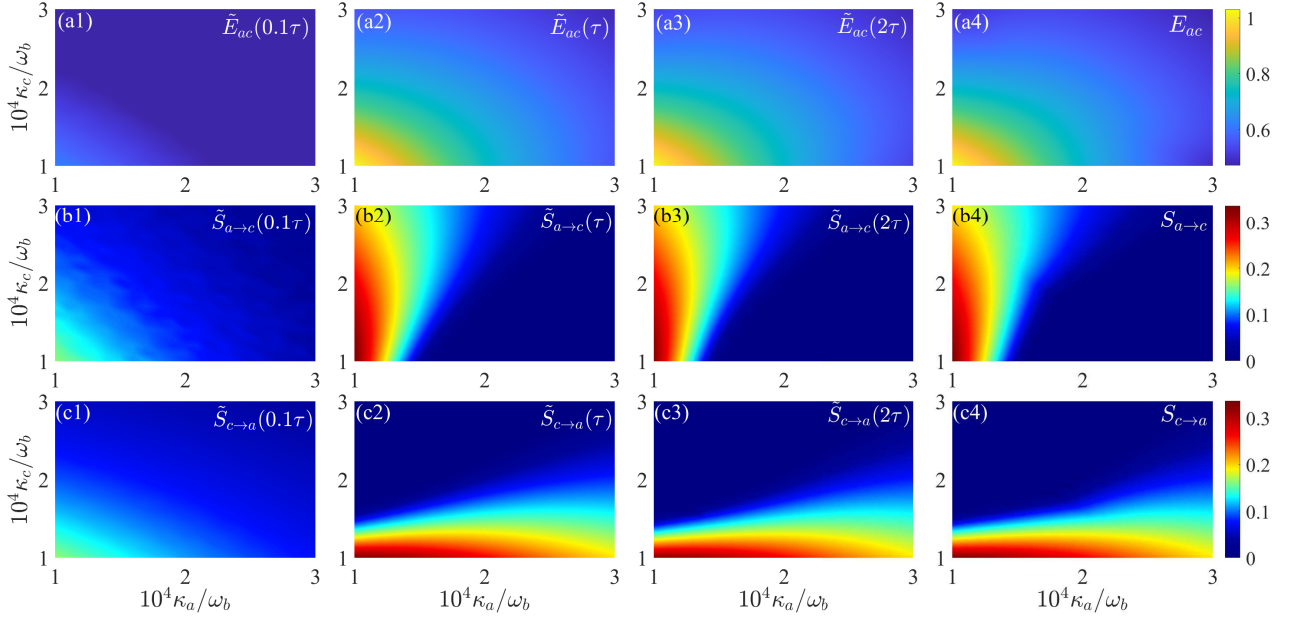


FIG. S9. The performance of MO entanglement \tilde{E}_{ac} (a) and quantum steering $\tilde{S}_{a \rightarrow c}$ (b) and $\tilde{S}_{c \rightarrow a}$ (c) in the decay rates κ_a and κ_c space at times 0.1τ , τ , and 2τ , respectively, in agreement with the corresponding theoretical predictions at $t \rightarrow \infty$. The parameters are set as $g_a = g_c = 0.12\omega_b$, $g_m = 0.1\omega_b$, $\Delta_m = \omega_b$, $\Delta_a = 3\omega_b$, $\kappa_m = 10^{-3}\omega_b$, $\kappa_b = 10^{-6}\omega_b$, $N_a = N_m = N_c = 0$, and $N_b = 10$.

with theory. Figure S10 presents theoretical and numerical results at the characteristic time τ versus the detuning Δ_m , showing good agreement in both steady-state and most unsteady-state regimes, consistent with Eq. (S21). As Δ_m increases, the quantum resources are enhanced, and the system undergoes a transition from one-way to two-way steering. Moreover, $\tilde{E}_{ac}(\tau)$ [$\tilde{S}_{a \rightarrow c}(\tau)$] exhibits a slight deviation from the corresponding theoretical prediction E_{ac} ($S_{a \rightarrow c}$) when $\Delta_m \gtrsim 1.5\omega_b$, since the perturbative validity condition $g_a, g_c, g_m \ll |\Delta_a - \Delta_m|$ is no longer satisfied for $\Delta_a = 3\omega_b$.

In the COMM system [5], the enhanced coupling strengths g_m and g_c , as well as the detunings Δ_a , Δ_c , and Δ_m , can

be precisely controlled via the microwave driving field and optical laser. The effective coupling strength depends on both the couplings and detunings, as given by Eq. (S53). The mechanical frequency is typically in the range of 10–100 MHz, with a decay rate of $\kappa_b/\omega_b \sim 10^{-6}$ [5, 6]. The decay rates of the magnon, microwave, and optical modes are $\kappa_m, \kappa_a, \kappa_c \sim 10^{-4} - 10^{-3}\omega_b$ [5–7], respectively. The microwave-magnon, magnomechanical, and optomechanical coupling strengths are $g_a, g_m, g_c \sim 0.1\omega_b$ [5], allowing the unsteady-state condition $g_{\text{eff}}^2 > \kappa_a \kappa_c$ to be readily achieved. At low temperatures ($T \sim 10$ mK), the thermal excitation numbers of all microwave magnon and optical modes are negligible, while the mechanical mode has $N_b \sim 10$ [5].

IV. MULTIPARTITE ENTANGLEMENT AND STEERING

In multipartite quantum systems, quantum resources such as entanglement and quantum steering are constrained by monogamy relations and cannot be freely shared [8, 9]. In this section, we analyze the distribution of quantum resources in hybrid quantum systems within the validity regime of the effective Hamiltonian.

At first, we quantify the quantum entanglement between a single mode a and remaining modes B in a hybrid quantum system using the LN [1]. The definition of single-vs-multipartite LN $E_{a|B}(t)$ is given by

$$E_{a|B}(t) = \max [0, -\ln(2\eta_{a|B}^-)], \quad (\text{S58})$$

where $B \equiv b_1 \dots b_s \dots b_{N_c}$, $\eta_{a|B}^- = \min(\text{eig}[i\sigma\tilde{v}])$ is the smallest symplectic eigenvalue. Here, $\sigma = \bigoplus_1^{N+2} i\sigma_y$

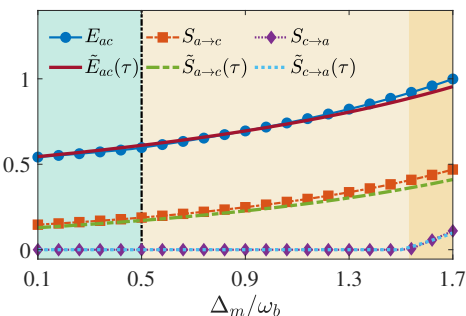


FIG. S10. Theoretical predictions and numerical results for the MO entanglement \tilde{E}_{ac} and quantum steering $\tilde{S}_{a \rightarrow c}$ and $\tilde{S}_{c \rightarrow a}$ versus the detuning Δ_m . The black dot-dashed line indicates the boundary between the steady-state (left) and unsteady-state (right) regimes. $\kappa_a = 0.5\kappa_c = 10^{-4}\omega_b$ and the other parameters are the same as Fig. S9.

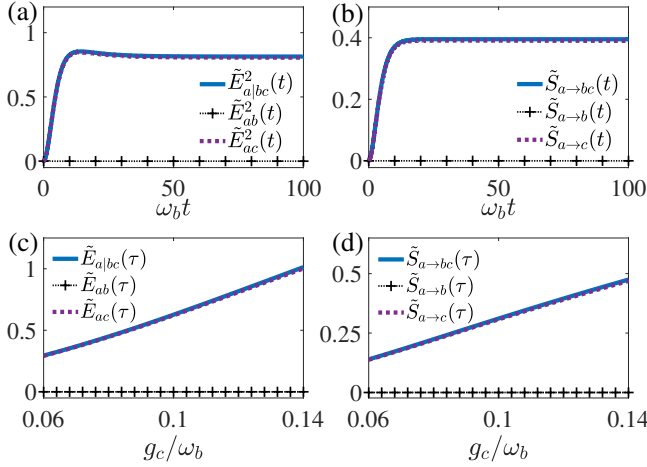


FIG. S11. Time evolution of the entanglement (a) and quantum steering (b) for $g_c = 0.12\omega_b$, and efficient quantum control of the MO entanglement (c) and quantum steering (d) versus the coupling strength g_c , in the EOM system. Other parameters are the same as those in Fig. S5(a).

with σ_y denoting the y -Pauli matrix. $\tilde{v} = P_{a|B}vP_{a|B}$, where v represents the CM of whole system and $P_{a|B} = \text{diag}(1, -1, 1, 1, \dots, 1, 1)$. Similarly, the criterion [2] to measure the Gaussian quantum steering between single-mode and multi-modes is given by

$$S_{a \rightarrow B}(t) = \max[0, -\ln(2\mu_{aB})], \quad (\text{S59})$$

where μ_{aB} is the minimum symplectic eigenvalue of the matrix ν , which is the Schur complement matrix of v_a in the CM $v = [v_a v_{aB}; v_{aB}^T v_B]$, defined as $\nu = v_B - v_{aB}^T v_a^{-1} v_{aB}$. When subsystem B is a single mode, Eq. (S59) reduces to the same result as Eq. (S17) [2].

Both entanglement and quantum steering are constrained by monogamy relations. Specifically, the entanglement satisfies the Coffman-Kundu-Wootters (CKW)-type monogamy inequality [8, 9]

$$E_{a|B}^2 - \sum_{s=1}^N E_{ab_s}^2 - E_{ac}^2 \geq 0, \quad (\text{S60})$$

where $E_{a|p}$ is the entanglement between mode a and mode p ($p = b_s, c, B$). Similarly, the quantum steering obeys

$$S_{a \rightarrow B} - \sum_{s=1}^N S_{a \rightarrow b_s} - S_{a \rightarrow c} \geq 0, \quad (\text{S61})$$

where $S_{a \rightarrow B}$ denotes the multi-mode steering from mode a to the set of other modes, and $S_{a \rightarrow b_s}$ ($S_{a \rightarrow c}$) represent the steering from mode a to mode b_s (c).

We analyze the distributions of entanglement and quantum steering among different bipartitions of the EOM system. In Figs. S11(a) and (b), the time evolution of these distributions is shown for $g_c/\omega_b = 0.12$. The results indicate that dynamically stable bipartite entanglement and quantum steering

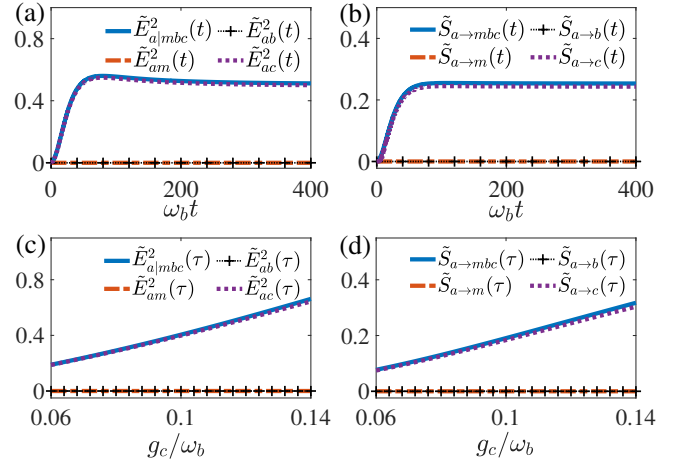


FIG. S12. Time evolution of the entanglement (a) and quantum steering (b), and efficient quantum control of the MO entanglement (c) and quantum steering (d) versus the coupling strength g_c , in the COMM system, where the decay rates are $\kappa_a = 0.5\kappa_c = 10^{-4}\omega_b$, and other parameters are the same as those in Fig. S9.

can be established, with $E_{ac}^2(t) \approx E_{a|bc}^2(t)$ and $S_{a \rightarrow c}(t) \approx S_{a \rightarrow bc}(t)$ throughout the entire time evolution, while all other bipartite resources remain negligible. In Figs. S11(c) and (d), the entanglement and quantum steering distributions at the characteristic time τ are plotted versus the relative coupling strength g_c/ω_b . The values of $\tilde{E}_{ac}^2(\tau)$ [$\tilde{S}_{a \rightarrow c}(\tau)$] closely approach those of $\tilde{E}_{a|bc}^2(\tau)$ [$\tilde{S}_{a \rightarrow bc}(\tau)$], whereas the other resources remain negligibly small.

We also investigate the distribution of entanglement and quantum steering among different bipartitions of the COMM system. Figures S12(a) and (b) show the dynamical evolution of these distributions for $g_c/\omega_b = 0.12$. The results indicate that dynamically stable bipartite entanglement and quantum steering can be established, satisfying $E_{ac}^2(t) \approx E_{a|mbc}^2(t)$ and $S_{a \rightarrow c}(t) \approx S_{a \rightarrow mbc}(t)$, whereas the remaining bipartite contributions are consistently negligible throughout the evolution. Figures S12(c) and (d) further show the dependence of the entanglement and quantum steering distributions on the relative coupling strength g_c/ω_b at the characteristic time τ . The values of $\tilde{E}_{ac}^2(\tau)$ [$\tilde{S}_{a \rightarrow c}(\tau)$] closely approach those of $\tilde{E}_{a|mbc}^2(\tau)$ [$\tilde{S}_{a \rightarrow mbc}(\tau)$], while all the other quantum resources remain negligible.

[1] G. Adesso and F. Illuminati, *Entanglement in continuous-variable systems: recent advances and current perspectives*, *J. Phys. A: Math. Theor.* **40**, 7821 (2007).

[2] I. Kogias, A. R. Lee, S. Ragy, and G. Adesso, *Quantification of Gaussian Quantum Steering*, *Phys. Rev. Lett.* **114**, 060403 (2015).

[3] S. Barzanjeh, M. Abdi, G. J. Milburn, P. Tombesi, and D. Vitali, *Reversible Optical-to-Microwave Quantum Interface*, *Phys. Rev. Lett.* **109**, 130503 (2012).

[4] S. Barzanjeh, S. Guha, C. Weedbrook, D. Vitali, J. H. Shapiro, and S. Pirandola, *Microwave Quantum Illumination*, *Phys. Rev. Lett.* **114**, 080503 (2015).

[5] Z.-Y. Fan, L. Qiu, S. Gröblacher, and J. Li, *Microwave-Optics Entanglement via Cavity Optomagnomechanics*, *Laser Photonics Rev.* **17**, 2200866 (2023).

[6] M. Aspelmeyer, T. J. Kippenberg, and F. Marquardt, *Cavity optomechanics*, *Rev. Mod. Phys.* **86**, 1391 (2014).

[7] B. Zare Rameshti, S. Viola Kusminskiy, J. A. Haigh, K. Usami, D. Lachance-Quirion, Y. Nakamura, C.-M. Hu, H. X. Tang, G. E. Bauer, and Y. M. Blanter, *Cavity magnonics*, *Phys. Rep.* **979**, 1 (2022).

[8] T. Hiroshima, G. Adesso, and F. Illuminati, *Monogamy Inequality for Distributed Gaussian Entanglement*, *Phys. Rev. Lett.* **98**, 050503 (2007).

[9] L. Lami, C. Hirche, G. Adesso, and A. Winter, *Schur Complement Inequalities for Covariance Matrices and Monogamy of Quantum Correlations*, *Phys. Rev. Lett.* **117**, 220502 (2016).